

A Radial Velocity Survey of the Cygnus OB2 Association

Daniel C. Kiminki¹, Henry A. Kobulnicky¹, K. Kinemuchi¹, Jennifer S. Irwin², Christopher L. Fryer^{3,4}, R. C. Berrington¹, B. Uzpen¹, Andy J. Monson¹, Michael A. Pierce¹, S. E. Woosley⁵

ABSTRACT

We conducted a radial velocity survey of the Cygnus OB2 Association over a 6-year (1999 – 2005) time interval to search for massive close binaries. During this time we obtained 1139 spectra on 146 OB stars to measure mean systemic radial velocities and radial velocity variations. We spectroscopically identify 73 new OB stars for the first time, the majority of which are likely to be Association members. Spectroscopic evidence is also presented for a B3Iae classification and temperature class variation (B3 – B8) on the order of 1 year for Cygnus OB2 No. 12. Calculations of the initial mass function with the current spectroscopic sample yield $\Gamma = -2.2 \pm 0.1$. Of the 120 stars with the most reliable data, 36 are probable and 9 are possible single-lined spectroscopic binaries. We also identify 3 new and 8 candidate double-lined spectroscopic binaries. These data imply a lower limit on the massive binary fraction of 30% – 42%. The calculated velocity dispersion for Cygnus OB2 is $2.44 \pm 0.07 \text{ km s}^{-1}$, which is typical of open clusters. No runaway OB stars were found.

Subject headings: techniques: radial velocities — binaries: general — binaries: spectroscopic — binaries: close — stars: early-type — stars: kinematics — surveys

1. Introduction

Cygnus OB2 may be one of the most massive and richest associations in the Galaxy with 2600 ± 400 OB cluster members (Knödlseider 2000, hereafter Kn00) and 90 to 100 O

¹Dept. of Physics & Astronomy, University of Wyoming, Laramie, WY 82070

²Department of Astronomy and McDonald Observatory, University of Texas, Austin, TX 78712

³Theoretical Astrophysics, Los Alamos National Laboratories, Los Alamos, NM, 87545

⁴Department of Physics, The University of Arizona, Tucson, AZ 85721

⁵Department of Astronomy & Astrophysics, University of California Santa Cruz, Santa Cruz, CA, 95064

stars (Comerón et al. 2002, Kn00). It has been studied numerous times due to its richness, proximity (1.7 kpc — Hanson (2003); Massey & Thompson (1991); Schulte (1958); Johnson & Morgan (1954)), and high extinction components with $A_V > 5$. The total mass of the cluster is estimated to be $(4 - 10) \times 10^4 M_\odot$ with a central stellar density of $\rho_0 = 40 - 150 M_\odot pc^{-3}$ (Kn00). The radius of Cyg OB2 has been estimated as large as 30 pc (Kn00). For the purposes of this study, we adopt a cluster core radius of ~ 15 pc ($30'$) inferred from the photometric survey of Massey & Thompson (1991, hereafter MT91).

A handful of massive binaries have been discovered in the Association. Among the OB type binaries are MT421, MT429, MT506, MT554, MT696, Cyg OB2 No. 5, and Cyg OB2 No. 8a (MT465). The first four of these are eclipsing binaries of the Algol type (Pigulski & Kolaczowski 1998; Kazarovets et al. 2000). Rios & DeGioia-Eastwood (2004) discovered that MT696 is an early contact binary (W UMa type) consisting of a late O and an early B star with a period of 1.46 days. Cyg OB2 No. 5 is possibly a triple system consisting of an O7Iafp + Ofpe/WN9 contact binary with period of 6.6 days (Leung & Schneider 1978) and a B0V star (Benaglia et al. 2001; Walborn 1973; Bohannan & Conti 1976). Cygnus OB2 No. 8a is a non-thermal radio emitter (Bieging et al. 1989) and massive binary system consisting of O6 and O5.5 stars with a period of ~ 22 days (De Becker et al. 2004).

Massive close binaries (MCB) are the progenitors of some classes of energetic phenomena such as supernovae, γ -ray bursts, and X-ray binaries (Fryer et al. 1999, 1998). They are also laboratories in which to study the formation mechanisms for massive stars (Bonnell et al. 1998). Direct and indirect evidence reveals that up to 50 – 80% of massive stars reside in binary systems (Vanbeveren 2004; Gies 1987; Garcia & Mermilliod 2001). Studies of the MCB frequency are numerous and include Hillwig et al. (2006), Vanbeveren (2004), Zinnecker (2003), Garcia & Mermilliod (2001), Bonnell et al. (1998), Van den Heuvel & Van der Woerd (1983), and Garmany et al. (1980). Results have been all but conclusive. The binary frequency for Galactic B0 – B3 stars is at least 32%, and it may be anywhere between 14% and 80% for OB stars in general (Vanbeveren 2004; Vanbeveren et al. 1998; Garcia & Mermilliod 2001). In addition, Vanbeveren (2004) speculates that there may not be a standard MCB frequency for open clusters and associations. The long term goal of this study is to provide a measurement of the MCB frequency, binary star mass ratios and orbital separations of Cygnus OB2 stars.

Section 2 presents our observations and data reduction. Section 3 discusses the identification of new early type stars and our derivations of cluster quantities such as the initial mass function, visual extinction, and distance. Section 4 describes the calculation of radial velocities. Section 5 presents the results and a measurement of the cluster velocity dispersion. Section 6 summarizes the survey findings.

2. Observations

Between 1999 July and 2005 October we observed 183 stars in the direction of the Cygnus OB2 Association with the echelle spectrographs at the Lick 3 m and Keck¹ 10 m telescopes, the Hydra spectrograph at the WIYN² 3.5 m telescope, the Wyoming Infrared Observatory (WIRO) fiber-bundle spectrograph (WIRO-spec; Nations & Pierce (2002)) and the WIRO Longslit spectrograph at the WIRO 2.3 m telescope. Table 1 lists the observing runs at each facility and the approximate spectral coverages. Stars were selected from the UBV photometric and spectroscopic survey of Cyg OB2 by MT91. We included 73 stars with previous spectroscopic OB classification from Table 5 of MT91. During the initial 1999 Keck run we included 110 additional stars from MT91 having reddening-free parameter $Q \equiv (U - B) - 0.8(B - V)$ corresponding to stars earlier than $\sim B3$. Our motivation was to obtain a more complete sample of reddened early type stars. However, this more inclusive sample necessarily contained foreground A – G stars and background or foreground OB stars.

At the Lick 3 m telescope, the Hamilton echelle spectrograph was used to cover the wavelength range $\lambda 3620 \text{ \AA}$ to $\lambda 7675 \text{ \AA}$ in 82 spectral orders with a mean spectral resolution of $R \sim 30,000$. These observations occurred over eight nights, 1999 July 21 – 23, 1999 August 21 – 23, and 2000 July 10 – 11. Exposure times ranged between 240 and 1200 seconds. Hourly exposures of a Thorium-Argon served to calibrate the wavelength of each exposure to an RMS of 0.002 \AA (0.12 km s^{-1} at 5000 \AA). The typical resolution was 0.12 \AA FWHM at $\lambda 5700 \text{ \AA}$ and 0.08 \AA FWHM at $\lambda 3700 \text{ \AA}$. A $1.2'' \times 2.5''$ slit decker was used throughout. Observations of six radial velocity standard stars were used to confirm the repeatability of the wavelength calibration from epoch to epoch.

We acquired spectra at Keck with the HIRES spectrograph (Vogt et al. 1994) on 1999 July 4-5, 1999 October 18-19, and 2000 September 14-15. We used the blue collimator to obtain $R \sim 30,000$ spectra over the wavelength range $\lambda 3600 - 5200 \text{ \AA}$ ($\lambda 3900$ to $\lambda 5800 \text{ \AA}$ on the 1999 July 4-5 run). On the 1999 July run, spectral regions from $\lambda 5163 - 5172 \text{ \AA}$ and $\lambda 5238 - 5246 \text{ \AA}$ are unusable due to blemishes on the detector, while on the other Keck runs, spectral regions $\lambda 4512 - 4517 \text{ \AA}$ are unusable. The slit decker C5 measuring $1.15''$ in the spectral direction and $7.0''$ in the spatial direction was used throughout. Periodic exposures of a Thorium-Argon arc lamp were used to calibrate the radial velocity of the spectra which

¹The W.M. Keck Observatory is operated as a scientific partnership among the California Institute of Technology, the University of California and the National Aeronautics and Space Administration. The Observatory was made possible by the generous financial support of the W.M. Keck Foundation.

²The WIYN Observatory is a joint facility of the University of Wisconsin-Madison, Indiana University, Yale University, and the National Optical Astronomy Observatory.

were then tied to radial velocity standards. The wavelength scale of each exposure is good to an RMS of 0.003 \AA (0.18 km s^{-1} at 5000 \AA). The output pixel scale is $\sim 0.04 \text{ \AA/pix}$. The mean instrumental resolution was 0.12 \AA FWHM at $\lambda 5000 \text{ \AA}$ and 0.09 \AA FWHM at $\lambda 3700 \text{ \AA}$.

At WIYN we used the Hydra spectrograph with the Red camera, $2''$ blue fibers, and the 1200 l/mm grating in second order to obtain three 1200 s exposures in each of three configurations (~ 90 stars each). The spectral coverage was $\lambda 3800$ to $\lambda 4500 \text{ \AA}$ at a mean resolution of $R \sim 4500$. Observations at WIYN took place over six nights, 2001 August 24, 2001 September 8-9, and 2004 November 28-30. Helium-Neon-Argon lamps were used between each exposure to calibrate the spectra to an RMS of 0.03 \AA (2 km s^{-1} at 4500 \AA), and the typical resolution was 1.0 \AA FWHM at $\lambda 3900 \text{ \AA}$ and 0.82 \AA FWHM at $\lambda 4400 \text{ \AA}$.

At WIRO we used the WIRO-Spec fiber bundle spectrograph with 15×20 fiber array and $1''$ fibers to achieve $R \sim 4500$ over the wavelength range $\lambda 4075 - 4910 \text{ \AA}$ at a dispersion of 0.41 \AA/pix . Observations at WIRO occurred over eight nights, 2005 July 18-21, and September 18-20, & 22. Copper-Argon lamp exposures were used every 30 minutes to wavelength calibrate the spectra to an RMS of $0.1\text{-}0.2 \text{ \AA}$ ($6.7 - 13 \text{ km s}^{-1}$ at 4500 \AA). The mean spectral resolution was 0.98 \AA FWHM at $\lambda 4500 \text{ \AA}$. Typically, three to five 600 s exposures were obtained for each object. At WIRO, only a handful of the brightest stars with previously discovered large-amplitude velocity variations were observed.

We also obtained spectra of the seven brightest stars exhibiting large velocity variations with the WIRO longslit spectrograph on 2005 October 13. We used a $2.5''$ slit width. The spectra covered the wavelength range $\lambda 3950$ to $\lambda 6050 \text{ \AA}$ at a dispersion of 1.12 \AA/pix . Argon lamps were used to calibrate the spectra to an RMS of 0.15 \AA (10 km s^{-1} at 4500 \AA). The mean spectral resolution was 3.2 \AA FWHM at $\lambda 4500 \text{ \AA}$. Two or three 600 s exposures were acquired for each object.

The data were reduced in IRAF using standard data reduction techniques which included flat fielding with exposures of an internal or dome quartz continuum lamp. One dimensional spectra were extracted and wavelength calibrated by interpolating a wavelength solution determined from periodic exposures of the arc lamps throughout the night. At each observatory and instrument, the variation in the wavelength solution during the night was small ($< 0.5 \text{ \AA}$), monotonic, and well constrained by the frequent arc calibration. Because many of the nights were not photometric, no attempt at flux calibration was made. The one dimensional spectra were corrected to a heliocentric velocity scale by computing the appropriate Doppler correction for each source, date, time of observation, and observatory using IRAF tasks RVCOR and DOPCOR. Similar spectra from a given night were then combined, weighted by the signal to noise. The final signal-to-noise ratios vary with wavelength, magnitude, telescope, instrument, and observing run. They range from $150:1$ per pixel near

4400 Å for WIYN observations of the brightest stars to 5:1 for some of the Lick data where intermittent clouds affected the data.

Observations of the radial velocity standard stars HD012929 (SpT: K2III), HD171391 (G8III), HD182572 (G8IV), HD187691 (F8V), HR1320 (B2IV), HD1174 (B3V) were obtained on the Lick and Keck nights as a check on the wavelength calibration. Inspection of the corrected radial velocity standard star spectra shows excellent agreement between all epochs, giving confidence that the data are free from systematic velocity offsets between epochs and telescopes. The epoch-to-epoch velocity dispersion among velocity standards after correction to the heliocentric reference frame is 0.05 Å ($\sim 3 \text{ km s}^{-1}$), i.e., less than the instrumental resolution.

The current dataset includes 1139 individual spectra obtained over 29 epochs for 183 stars, 146 of which are OB stars. The mean number of observations per star was 7, the median was 6, minimum was 1, and the maximum was 19.

3. New Spectral Classifications and Derived Quantities

We estimated new spectral types for all stars by visual comparison with the stellar atlas of Walborn & Fitzpatrick (1990). Table 2 provides a list of all OB stars in our survey using the nomenclature of MT91. Columns 2 and 3 list spectral types from the literature for each object (primarily from MT91; see their Table 5) and as determined by our survey, respectively. Spectral types were determined independently by two authors, with the exception of Cygnus OB2 No. 12, and there was generally good agreement to within one spectral class. Of the 110 stars without previous spectral classifications, 73 were OB stars, while 37 were A or later. These 37 non-OB stars are listed in Table 3 and range from A to M.

3.1. Cygnus OB2 No. 21

Two thoroughly observed stars, Cyg OB2 No. 12 and No. 21, exhibited large discrepancies between our new spectral type and those listed in the literature. Torres-Dodgen et al. (1991) spectroscopically classify Cygnus OB2 No. 21 (MT259) as a B1 and photometrically as B1V. MT91 also classified this star a B1V. Spectra of all epochs obtained on MT259 were consistent, and we find that this star is best represented by a B0Ib spectral classification. In Figure 1 we present a spectrum of MT259 taken on 2001 September 9 at the WIYN observatory. The most distinguishing feature of this star’s spectrum is the large number of metal lines, especially around $H\delta \lambda 4101 \text{ Å}$. Figure 1 also shows the spectra of HD164402 (B0Ib)

and HD144470 (B1V) from the Walborn & Fitzpatrick (1990) spectral atlas for comparison.

3.2. Cygnus OB2 No. 12

Cygnus OB No. 12 (MT304) is one of the most notable stars in the Association. It holds the reputation as one of the most luminous and reddened objects in the Galaxy (Sharpless 1957; Johnson 1968). It is also a bright x-ray source (Harnden et al. 1979) and variable radio emitter (Setia Gunawan et al. 2003). The X-ray emission is best explained by wind driven shocks (Waldron et al. 2004), where No. 12 has a measured high stellar wind of $V_{WIND} = 1400 \text{ km s}^{-1}$ (Leitherer & Wolf 1982; Bieging et al. 1989), and an expanding shell of $V = 3100 \text{ km s}^{-1}$ (Wang & Zhu 2003). It has been shown to vary photometrically (Gottlieb & Liller 1978; Voelcker 1975), and Souza & Lutz (1980) submit that a binary companion may provide an explanation for this. MT91 suggest the possibility that No. 12 is a Luminous Blue Variable because it appears to vary spectroscopically as well as photometrically and has an extremely high luminosity.

Most studies adopt a spectral type for No. 12 of B5Iae (MT91) or B8Iae (Souza & Lutz 1980). Abbott et al. (1981) adopt B3Iae but little justification for such an early classification is found in the literature. We find evidence for a B3Iae spectral type and a temperature class variation between B3 and B8 by comparison with the OB star atlas of Walborn & Fitzpatrick (1990), the supergiant atlas of Lennon et al. (1992), and the spectral atlas of Yamashita & Nariari (1977). Figure 2 presents segments of the spectrum obtained on 2000 September at Keck. Panel 1 shows the temperature-sensitive ratio He I $\lambda 4471 \text{ \AA}$ to Mg II $\lambda 4481 \text{ \AA}$, the strongest evidence for a B3Iae spectral type. Mg II is a weaker feature than He I for temperature classes earlier than B7 and is stronger than He I for a B8 class or later. The observed ratio is approximately 2:1, characteristic of a B3 temperature class. It should be noted that the spectrum presented by Souza & Lutz (1980) shows a ratio characteristic of a B8 class (Souza & Lutz 1980, Figure 1), and the spectrum presented by MT91 shows a ratio characteristic of B3 (although it is reported as B5 due to additional arguments; see Figure 12 in MT91). The presence of the absorption feature $\lambda 4542 \text{ \AA}$ (Panel 2) provides additional evidence for a B3 classification. The relative intensity and asymmetric profile of the absorption suggests a blend of the two lines He II $\lambda 4542 \text{ \AA}$ and Fe II $\lambda 4542 \text{ \AA}$. This is generally only seen in the earliest of B stars. Panel 3 shows H β $\lambda 4861 \text{ \AA}$, He I $\lambda 4922 \text{ \AA}$, and a weak Fe II $\lambda 4923$. The strength of the He I absorption in relation to the weak Fe II absorption suggests an earlier type. Panel 4 shows an example of deep absorption in one of the higher ionization lines, N III $\lambda 4097 \text{ \AA}$. There is also a possible He II feature at $\lambda 4100 \text{ \AA}$, next to H δ $\lambda 4101 \text{ \AA}$. We see additional evidence for weak He II absorption toward the blue

end of the spectrum (i.e., $\lambda 3710 \text{ \AA}$ and $\lambda 3720 \text{ \AA}$). The absence of Si IV $\lambda 4089 \text{ \AA}$ suggests a classification no earlier than B3. Panels 1 and 4 also display clear examples of documented emission-line cores in No. 12 (He I $\lambda 4471 \text{ \AA}$ and N III $\lambda 4097 \text{ \AA}$).

Fluctuations in the spectrum of No. 12 are seen in our 2001 August and September spectra obtained at WIYN and are shown in Figure 3. Souza & Lutz (1980) noted small spectral fluctuations in their spectra over a time scale of days. Figure 3 shows three of our spectra obtained over the span of one year and demonstrates a temperature class evolution between B3 and B8. The upper spectrum is from Keck HIRES on 2000 September 18, and the lower two spectra are from WIYN Hydra on 2001 August 24 and September 9. The broad interstellar band feature near 4428 \AA is absent in the high-resolution Keck spectrum because it has been fitted and removed during continuum normalization. The ratio of He I $\lambda 4471 \text{ \AA}$ to Mg II $\lambda 4481 \text{ \AA}$ changes from over 2:1 to near 1:1. The strength of the Si II $\lambda 4128 \text{ \AA}$ & $\lambda 4130 \text{ \AA}$ doublet becomes stronger than the adjacent He I lines. N III $\lambda 4097 \text{ \AA}$ becomes noticeably weaker than H δ $\lambda 4101 \text{ \AA}$ and Fe II $\lambda 4232 \text{ \AA}$ becomes much stronger. In addition, the Balmer line strength also increases. Emission in the Balmer and higher ionization lines is also less dominant in the 2001 August and September spectra which are best described by a classification of B6 and B8. It is more dominant in the 2000 September spectrum which is best described by a classification of B3. A sign of late B classification is the appearance of the Mg I doublet at $\lambda 5173 \text{ \AA}$ and $\lambda 5184 \text{ \AA}$, however the August and September WIYN spectra did not cover this section of the spectrum and the Keck spectrum showed no evidence of them. The Lick data did cover this spectral range but were not of sufficient S/N for detailed classification.

3.3. Visual Extinction and Distance

Table 2 provides the calculated visual extinctions (Column 6) and distance moduli (column 13) for the 146 OB stars in the direction of Cyg OB2. The values were calculated from apparent visual magnitudes (Column 7), absolute visual magnitudes (Column 8), colors, $(B - V)$ (Column 9), and intrinsic colors, $(B - V)_0$ (Column 10). The apparent visual magnitudes and $(B - V)$ colors were obtained from MT91. The absolute visual luminosities were adopted from Martins et al. (2005) for the O stars and Humphreys & McElroy (1984) for the B stars. The intrinsic $(B - V)_0$ colors were based on adopted spectral types and obtained from Wegner (1994).

We computed the visual extinctions, A_V , using

$$A_V = R_V[(B-V) - (B-V)_0], \quad (1)$$

where R_V is the ratio of total to selective extinction. We adopt $R_V = 3.0$ based on the studies of Hanson (2003) and MT91. Visual extinctions range between $A_V = 3.5$ and $A_V = 10.4$ (for No. 12) with a mean near $A_V = 5.4$ mag, consistent with prior results (e.g., MT91). Figure 4 shows an extinction map for all OB stars in the direction of Cygnus OB2 where the relative symbol size is proportional to A_V . Using these calculated extinctions, we computed photometric distance moduli to all of the OB stars using

$$DM = V - M_V - A_V, \quad (2)$$

where V is the apparent visual magnitude and M_V is the absolute visual magnitude. Figure 5 shows a histogram of the computed distance moduli for all 146 OB stars in the direction of Cyg OB2. This histogram peaks at $D. M. \simeq 11.3$ magnitudes or $\simeq 1.8$ kpc, in good agreement with the commonly adopted distance estimate of 1.7 kpc (Hanson 2003; Massey & Thompson 1991; Schulte 1958). The distribution is approximately Gaussian with a width of $\sigma=1.0$ mag. The large width reflects the uncertainties on the absolute visual magnitudes, particularly for evolved stars, and uncertainties in temperature and luminosity classification. Hanson (2003) found a similar scatter in DM of up to 1.5 mag and mean distance moduli from 10.08 – 11.16 mag, depending on the adopted absolute magnitude calibrations. An additional systematic uncertainty arises from the presence of unresolved binaries which lead to smaller inferred distance moduli. Unresolved binaries are at least partially responsible for the asymmetry in the distribution in Figure 5. A third source of uncertainty might also stem from the ratio of total to selective extinction, R_V . Patriarchi et al. (2003) found an average $R_V = 3.1$ for the Cygnus region, but a spread of ~ 1 . A spread of 1 in R_V translates to a spread in A_V of approximately 1 – 2 magnitudes for our sample. The compound extinction components in combination with the density of documented O stars in Cygnus OB2 could create conditions under which the dust grain size distribution and composition vary and lead to a variable R_V across the cluster.

3.4. New Early Types and Cluster Membership

The true distance moduli shown in Figure 5 are listed in column 13 of Table 2. For the purposes of this study, we accept as provisional members all stars with distance moduli between $\sim 8.5 - 14.5$ mag which lie within the broad Gaussian distribution. Three stars fall outside of the distribution (MT427, MT573, and MT304). It will be shown in the following

section that including all such stars does not significantly affect the computed slope of the initial mass function. About half of these were previously identified spectroscopically as probable members by MT91. The other probable members were determined photometrically as a group by MT91 but not named individually. The total sample consists of 108 main sequence stars, 36 evolved stars and 2 with indeterminate luminosity class. We have identified 73 early type stars without previous spectral classification in the literature. Newly classified early type stars are denoted in column 14 of Table 2 with an ‘n’. Of these, 56 are main sequence stars, mostly type B0 and later.

As a secondary means of assessing membership for the early type stars, we examined the equivalent widths of the diffuse interstellar band (DIB) absorption feature at 4428 Å. We found that nearly all of the newly identified stars had $EW_{DIB} = 3 \pm 1$ Å, consistent with the established association members (Snow et al. 2002). Given the large spread in reddening and DIB equivalent width for Cyg OB2, and the fact that Snow et al. (2002) found a poor correlation between reddening and DIB strength for this cluster, we conclude that this relation is not a useful discriminant of members from field stars.

3.5. Initial Mass Function

Studies of the slope of the CygOB2 initial mass function have reached disparate conclusions. Kn00 used JHK 2MASS Point Source Catalog (Skrutski et al. 2006) photometry and a K-band mass-luminosity relation to calculate a mass function slope of $\Gamma = -1.6 \pm 0.1$. This is steeper than previous studies of Cyg OB2. MT91 utilized the evolutionary models of Maeder & Meynet (1988) with an H-R diagram constructed from their spectroscopy and “best” photometry to obtain a slope of $\Gamma = -1.0 \pm 0.1$. This is relatively shallow compared to the canonical Salpeter (1955) value of $\Gamma = -1.35$. Massey et al. (1995) found a similar slope of $\Gamma = -0.9 \pm 0.2$, using the same technique over a mass range of $15 M_{\odot} - 25 M_{\odot}$. In both calculations, a coeval system was assumed.

We calculated an IMF slope using the spectroscopic masses for the previously classified 73 OB stars and the 73 newly classified OB stars reported here. Present-day masses for each star were taken from Martins et al. (2005) for the O stars and interpolated from the tables of Drilling & Landolt (2000) for the B stars. Initial masses were also estimated for each of the evolved stars from the Lejeune & Schaerer (2001) stellar evolutionary models. Table 2 lists the present-day and adopted initial masses for each star in Columns 11 and 12. Figure 6 shows the cumulative logarithmic mass distribution of 143 Cyg OB2 stars with spectroscopic masses (minus Cygnus OB2 No. 12 owing to the uncertainty in its spectral type, mass loss rate, and current mass). We use a cumulative rather than a differential mass distribution to

measure the IMF slope in order to mitigate uncertainties caused by discrete mass bins and the choice of bin size and placement. Diamonds indicate the logarithmic number of stars with a logarithmic mass greater than or equal to that point. The error bars reflect Poisson statistics. It is clear from the change in slope at $\log(\text{mass}) \simeq 1.0$ that the spectroscopic survey becomes incomplete at masses below $\sim 15 M_{\odot}$ corresponding approximately to a B1V star. The solid line represents a linear fit to all points greater than this cutoff. We obtain a slope of $\Gamma = -2.2 \pm 0.1$. This is much steeper than the canonical Salpeter (1955) value of $\Gamma = -1.35$. This value is also steeper than the results of Kn00 and significantly more so than MT91. The possible inclusion of foreground or background stars may bias the slope toward steeper values. However, the IMF slope does not vary by more than 0.04 from the nominal value of $\Gamma = -2.20$ when we remove stars which lie farther than 1.5σ (24 stars) from the mean distance modulus of 11.3. The dominant explanation for the difference between our IMF and the previous results is a systematic difference in the predicted initial stellar masses between the models of Maeder & Meynet (1988, used by MT91) and Lejeune & Schaerer (2001, used in this study). The implied masses of Lejeune & Schaerer (2001) are systematically lower for a given bolometric luminosity and effective temperature compared to the models of Maeder & Meynet (1988). Effectively this means that we have fewer high-mass stars than MT91 which results in a steeper slope. We also calculated the slope of the present-day mass function (PDMF) to be $\Gamma = -2.3 \pm 0.1$, which is more appropriate for comparison to the photometric PDMF results of Kn00. It should also be noted that our sample is composed only of stars within the core of Cygnus OB2 while the Kn00 sample encompasses a large number of stars outside the core region.

4. Calculating the Relative Radial Velocities

We used two methods to calculate the relative and absolute radial velocities: Gaussian profile fitting and cross-correlation. For early type stars which have a small number of broad spectral features, profile fitting can be a reasonable approach. This method entailed fitting Gaussian profiles to the strong H and He absorption lines ($H\beta$, $H\gamma$, $H\delta$, He I $\lambda 4471$, and He I $\lambda 4388$). We used a five-parameter Gaussian³ of the form

$$f(x) = A_0 e^{-\frac{1}{2}(\frac{x-A_1}{A_2})^2} + A_4 x + A_3 \quad (3)$$

where A_0 is the *Depth*, A_1 is the *Center*, A_2 is the *FWHM*, A_3 is the *Constant Term*, and

³The IDL package “MPFIT” written by Craig B. Markwardt, NASA/GSFC Code 662, is substituted for the standard “GAUSSFIT” and “CURVEFIT” due to its greater control over the fitting parameters.

A_4 is the *Linear Term*. The code performs initial fits to the $H\beta$ and He I $\lambda 4471$ lines of a template spectrum (usually the highest quality Keck spectrum) in order to measure the widths of the H and He lines, respectively. The width parameter, A_2 , for the H and He lines is subsequently held constant at these initial values. The line centers are fixed relative to each other using the rest wavelengths from atomic line lists (Cowley et al. 2000). The code then fits profiles to all of the H and He lines with A_0 , A_3 , A_4 as free parameters for each line. The best-fit parameters are then saved and used to construct a “template” consisting of 5 Gaussian components. This template is then stepped through a range of velocities from -160 km s^{-1} to 160 km s^{-1} at a stepsize of 1 km s^{-1} to minimize the χ^2 between the template and spectra from each epoch. At each velocity step, A_0 , A_3 , and A_4 of each component are allowed to vary separately to achieve the best fit. The velocity of the global χ^2 minimum is adopted as the most probable velocity for each epoch. Because the H lines are stronger than the He lines, they were given more weight in the calculation of the total χ^2 . Spectra from WIYN have limited wavelength coverage and do not include $H\beta$, so only 4 Gaussian components are fit. Spectra from WIRO have limited wavelength coverage and do not include $H\gamma$, hence, only 4 Gaussian components are fit. Velocity uncertainties were calculated using the $\Delta\chi^2$ statistic (Press et al. 1986).

Gaussian fitting proved simple to automate for a large dataset. We also found it to be more robust for low signal-to-noise spectra and in regions at the edges of spectral orders in the echelle data. However, it often yielded larger uncertainties. We found that in the case of poor quality spectra the fitting routine would provide solutions for local or no minima.

We also measured radial velocities with cross-correlation techniques using the IRAF/XCSAO task which is part of the RVSAO package (Kurtz et al. 1991). This method had the advantage of using information in all spectral features, although for main sequence stars most of the cross-correlation power stems from the few strong H and He lines. As the template for cross-correlation we tried using both an observed spectrum (usually a high-quality Keck spectrum) and a model stellar atmosphere (Lanz & Hubeny 2003, TLUSTY) of the appropriate effective temperature and gravity. The model atmosphere is not rotationally broadened to match individual stars in our sample, but in the vast majority of cases the model line widths appear well-matched to the spectra. In most cases, the analysis using atmospheric model templates produced smaller velocity uncertainties than either the results from Gaussian fitting or cross-correlation with observed spectral templates. The smaller uncertainties result from the higher signal-to-noise of the model templates and the fact that this method uses the power of many additional spectral features in the templates and data to constrain radial velocities. Varying the gravity and effective temperature of the template produced little or no change in the correlation results. Therefore, we adopt the velocities obtained by cross-correlation with the model atmospheres. Table 4 contains the star name, heliocentric

Julian date, relative radial velocities, and 1σ error estimates for each epoch of observation in columns 1 – 4 respectively. The uncertainties are calculated within XCSAO using the equation,

$$\sigma_v = \frac{3w}{8(1+r)}, \quad (4)$$

where w is the FWHM of the correlation peak and r is the ratio of the correlation peak height to the amplitude of antisymmetric noise (Kurtz et al. 1991).

We found that the resultant relative radial velocities and their uncertainties showed good agreement between the two analysis methods. Figures 7 through 10 show comparisons of velocities and their uncertainties for an O8V, O9III, B0V, and B1I star respectively. These figures demonstrate that there is a strong correlation between velocities obtained with the fitting versus the cross-correlation techniques. Frequently, the error bars are smaller for the cross-correlation analysis, especially for evolved stars which have more spectral features that are utilized by cross-correlation methods but not by our Gaussian fitting code. Deviations from the 1:1 correspondence are generally consistent with the shown error, indicating that the statistical uncertainties are well-estimated. In most cases, there is also a zero-point offset of $\sim 10 - 15 \text{ km s}^{-1}$ in the sense that the profile-fitted velocities are smaller (i.e., more negative) than the results from cross-correlation. The magnitude of this offset is similar for both main-sequence and evolved stars. Such a modest offset is not unexpected given that the line centers of the model atmospheres should not necessarily agree with the rest wavelengths of the five H and He lines used by our profile fitting code.

From the initial sample of 146 possible Cyg OB2 stars, we discarded 26 stars from the sample that had fewer than 3 observations, poor quality spectra or emission lines that interfered with the cross-correlation analysis. The stars showing emission were discarded because the phenomenon might be time-variable and produce apparent radial velocity variations that mimic the effects of orbital motion. Furthermore, we eliminated a small number (~ 20 out of 1139) individual spectra with low signal-to-noise (mostly Lick data from a run plagued by clouds). The remaining sample used for velocity analysis consists of 120 stars.

For the remaining 120 objects, Table 5 lists the identification for each star based on MT91 notation (column 1), the spectral type (column 2), the number of observations for each star (column 3), V_{avg} , the weighted average heliocentric velocity (column 4), $V_{mid} \equiv 0.5(V_{max} + V_{min})$, the average of the largest and smallest observed heliocentric velocities (column 5), $V_h = 0.5(V_{max} - V_{min})$, a measure of the velocity semi-amplitude (column 6), V_{rms} , the velocity dispersion (column 7), and $\overline{\sigma}_v$, the mean velocity uncertainty (column 8). V_{avg} and V_{mid} are both measures of the systemic velocity for the star, although both

are susceptible in different ways to sampling effects and measurement errors. V_{avg} would provide a robust measure of the true systemic velocity if the observations uniformly sample all orbital phases in a binary system with zero eccentricity. However, our sparse sampling coupled with the likelihood that some orbits are eccentric renders this measure less than ideal. V_{mid} provides an alternative measure of the systemic velocity, which is less susceptible to under sampling but may be more prone to measurement uncertainty. We use both V_{avg} and V_{mid} as indicators of the systemic velocities, and we find that they yield comparable results. V_h and V_{rms} are both measures of the observed velocity variations for a given stellar system. V_h is a measure of the velocity semi-amplitude of the system, albeit an imperfect one, when the velocity curve is not sampled at all phases. V_{rms} is another measurement that reflects the level of velocity variations in a system. We use $\overline{\sigma}_v$ to describe a characteristic uncertainty averaged over all observations.

There is an additional source of random and/or systematic uncertainty which may contribute to the overall error budget of each measurement. Stellar photospheric line profile variations may be present among some of the most massive stars, especially the evolved stars in our sample (31 of 120 stars or about $\sim 26\%$ are post-main-sequence stars). Line profile variations attributed to atmospheric pulsations are observed in $\geq 77\%$ of evolved O stars and in some Be stars (Penrod 1986; Vogt & Penrod 1983) but rarely among dwarf stars (Fullerton et al. 1996). These phenomena could mimic the effects of bona fide orbital velocity variability. Irregular variability due to these effects might also mask a true low amplitude binary. More frequent time sampling of candidate variables is the only way to identify bona fide binaries and reduce mis-identification.

5. Results

5.1. Velocity Variations

Figure 11 shows a histogram of the observed radial velocities and mean uncertainties. This Figure illustrates the distribution of velocity dispersions, V_{rms} , calculated from the multiple measurements of the 120 OB stars (solid line) along with the distribution of mean velocity uncertainties, $\overline{\sigma}_v$ (dashed line). The dotted line shows the distribution of V_h . The lowest velocity bin from 0 to 5 km s⁻¹ is sparsely populated because observational errors scatter the data into higher velocity bins. The maximum observed semi-amplitudes fall mostly between 10 and 40 km s⁻¹, with a significant tail toward higher velocities out to ~ 90 km s⁻¹. The uncertainties lie in the characteristic range 5 – 15 km s⁻¹.

The velocity results in Table 5 show a wide range of characteristics, including stars

with large variations and stars with no significant variations. We used the method presented in Dequennoy & Mayor (1991) to identify probable spectroscopic variables in our survey. In Figure 12 we show the distribution of probabilities that χ^2 (as considered about the weighted mean of the measurements) would be exceeded given $\nu = N_{obs} - 1$ degrees of freedom. As in Dequennoy & Mayor (1991), the distribution is relatively flat except for values $P(\chi^2, \nu) \leq 0.01$. Column 9 of Table 5 lists the computed probabilities for the 120 stars examined. We identify in column 10 all stars with $P(\chi^2, \nu) \leq 0.01$ as probable SB1s (36 stars). In addition, we also identify the stars with $0.01 < P(\chi^2, \nu) < 0.04$ as possible SB1s (9 stars). The remaining objects are probable systems comprised of single stars, systems viewed at low inclinations, systems with very low mass companions or very long periods.

In Figures 13 through 16 we show heliocentric velocity versus time plots for four objects with minor or no velocity variations: MT083 (B1I; SB1), MT217 (O7II), MT264 (B2II), and MT317 (O8V). The data for most objects cover a time interval of ~ 5.5 years from 1999 July through 2004 November. The evolved systems among this group have some of the smallest velocity uncertainties in the survey ($< 5 \text{ km s}^{-1}$) and are particularly well suited to assess the level of possible systematic velocity errors from epoch to epoch. MT083 in particular (Figure 13) exhibits no epoch-to-epoch variations greater than $\sim 5 \text{ km s}^{-1}$ but has $P(\chi^2, \nu) < 0.0004$, indicating that it is a low-amplitude spectroscopic variable. This system also exhibits some photometric variability, raising the possibility that the velocity variations may be attributable to atmospheric activity (Kukarkin et al. 1981). In comparison with the small velocity variations present among these four objects, the magnitude of the Doppler correction due to the Earth’s orbital motion ranges from $\sim 8 \text{ km s}^{-1}$ in July to $\sim -16 \text{ km s}^{-1}$ in November. The constancy of the velocities, especially for evolved stars which have small uncertainties, among this subset of objects provides reassurance that systematic errors do not dominate the results.

Figures 17 through 22 show examples of some of the more prominent large-amplitude systems. In Figure 17, we present the velocity curve of MT059. This star exhibits large velocity variations of $\sim 100 \text{ km s}^{-1}$ with an average uncertainty of $\sim 11 \text{ km s}^{-1}$ on a timescale of ~ 3 days. Although our present data are not sufficiently time-sampled to uniquely determine the orbital parameters, these rough values imply a secondary mass of $\geq 7 M_{\odot}$ and an orbital separation of $\sim 0.12 \text{ AU}$ assuming an inclination near $i = 90^{\circ}$ and a circular orbit. Figure 18 shows MT138, an O8I star with an amplitude of nearly 85 km s^{-1} , an average uncertainty of $\sim 9 \text{ km s}^{-1}$, and variability on a several day timescale. These rough values imply a companion mass of $\geq 8 M_{\odot}$ and an orbital separation of $\sim 0.17 \text{ AU}$ assuming an inclination near $i = 90^{\circ}$. Figure 19 shows MT145, another evolved star (O9III). It has an amplitude of nearly 50 km s^{-1} and an average uncertainty of $\sim 4 \text{ km s}^{-1}$ with an apparent period of several days. The implied companion parameters are $M \geq 5 M_{\odot}$ and $a \simeq 0.15$

AU. Another O8V star (MT258) is presented in Figure 20. It displays an amplitude of at least 45 km s^{-1} and an average uncertainty of $\sim 10 \text{ km s}^{-1}$ with a period of several days. The implied companion parameters are $M \sim 3 M_{\odot}$ and $a \simeq 0.12 \text{ AU}$. MT492, a B1V in Figure 21 is representative of early B stars which have relatively few observations but still strong evidence for velocity variability. It has an amplitude of at least 50 km s^{-1} and an average uncertainty of $\sim 15 \text{ km s}^{-1}$. MT734, shown in Figure 22 is one of the brightest and most massive stars in the survey (O5I). We estimate an amplitude of $\sim 40 \text{ km s}^{-1}$, an average uncertainty of $\sim 7 \text{ km s}^{-1}$, and variations consistent with a period on the order of days. The implied companion parameters are $M \geq 4 M_{\odot}$ and $a \simeq 0.15 \text{ AU}$. At this time we can only make rough estimates of the orbital parameters for these few objects with the largest velocity amplitudes. Our present data, however, do not allow us to rule out short period aliases or non-periodic variations.

5.2. Double-Lined Spectroscopic Binaries

The cross-correlation analyses reveal 5 systems with double-lined spectra and 8 additional systems with possible double-lined signatures (3 of these are also designated SB1). These two groups are designated in column 10 of Table 5 as SB2 and SB2?, respectively. The latter group contains objects with variable cross-correlation widths, indicating possible multiplicity where the stellar features are blended at the resolution of the spectra. The former group contains objects where the velocity separation of the features is sufficient to allow the recognition of distinct spectral components at one or more epochs. Two of these systems are previously identified as SB2 in the literature: MT465 (De Becker et al. 2004) and MT696 (Rios & DeGioia-Eastwood 2004).

MT252 shows two velocity components in the He I and Mg I lines and variable width and asymmetry in the Hydrogen lines during two epochs (2001 September 8 – 9). The 2001 September 8 spectrum displays a maximum velocity amplitude of 101 km s^{-1} (He I) for both components, relative to the mean systemic velocity. This implies a mass ratio near unity. The ratio of luminosities of the two components is also near unity. Given the B1.5III spectral classification, this suggests the secondary is probably another B1.5III or possibly an O9V.

MT465 (Cyg OB2 No.8a) is reported to be a binary consisting of an O6 and an O5.5 star (De Becker et al. 2004). Despite the obvious double-lined spectra, 23-day period, and 200 km s^{-1} velocity separation reported in that work, the components are blended in all of our spectra. We therefore report this star as an SB1 and include an SB2 designation only because of the De Becker et al. (2004) study.

MT696, an O9.5V, is reported to be a double system containing an early-B secondary (Rios & DeGioia-Eastwood 2004). At least four of our observations of this star displayed dual velocity components in multiple lines. The ratio of velocity amplitudes is ~ 0.7 with a maximum velocity separation of 540 km s^{-1} on 2005 September 22. With a mass 70% of the O9.5V primary, the deduced secondary spectral type (B1/B2V) agrees with the findings of Rios & DeGioia-Eastwood (2004).

MT720, classified as an O9.5V, shows multiple velocity components, indicating that it is a probable triple system. The 2004 November 30 spectrum displays two velocity features with a separation of 350 km s^{-1} for the He I lines. The 2001 August 24 spectrum also shows two velocity components, but there is an additional asymmetry on the redshifted side of the H and He features. The 2001 September 9 spectrum clearly shows at least three velocity components in multiple lines. Luminosities amongst the primary, secondary, and tertiary are near unity and suggest comparable masses indicative of a system with three late-type O stars or B0 stars.

MT771, an O7V, shows He I double-lined components in three epochs (2001 September 9 and 2004 November 28–29), with a maximum velocity separation of 275 km s^{-1} . The ratio of velocity amplitudes is greater than 0.8 as measured about the systemic velocity calculated in the 2004 November 30 spectrum. The ratio of luminosities is ~ 0.75 , suggesting that the companion is a late O star.

5.3. Velocity Dispersion of Cyg OB2

Figure 23 provides histograms of systemic velocities for our two methods of velocity measurement. The shaded histogram represents the V_{mid} velocities in column 5 of Table 5. The unshaded histogram represents the V_{avg} velocities from column 4 of Table 5. A Gaussian fit to the data yields a FWHM of $8.01 \pm 0.26 \text{ km s}^{-1}$ for the shaded histogram and $5.7 \pm 0.17 \text{ km s}^{-1}$ for the unshaded histogram. This translates to a one dimensional radial velocity dispersion of $\sigma_V = 3.41 \pm 0.11 \text{ km s}^{-1}$ and $\sigma_V = 2.44 \pm 0.07 \text{ km s}^{-1}$ for V_{mid} and V_{avg} respectively. Both fits show that the mean systemic velocity of Cyg OB2 stars is $\bar{V}_{hel} = -10.3 \pm 0.3 \text{ km s}^{-1}$. Because the V_{mid} values have more outliers at large relative velocities, this measurement is best regarded as an upper limit to the true velocity dispersion. By comparison, typical open cluster velocity dispersions lie in the range $1 - 2.5 \text{ km s}^{-1}$ and may depend on initial conditions (Bate & Bonnell 1995). The velocity dispersions of other open clusters, such as the Orion nebula cluster (Jones & Walker 1988, 2 km s^{-1}), Perseus OB2 (Steenbrugge et al. 2003, $1 - 3 \text{ km s}^{-1}$), or Scorpius OB2 (de Bruijne 1999, $1.0 - 1.5 \text{ km s}^{-1}$), are consistent with our measurement of $V_{ave} = 2.44 \pm 0.07 \text{ km s}^{-1}$. We also examined

systemic velocity as a function of position within the cluster and found no evidence of large scale velocity patterns that might indicate the presence of kinematic subgroups.

5.4. Runaways in Cyg OB2

Nearly 20% of all O stars are runaways, with the other 70 – 80% locked in open clusters or OB associations (Kaper 1999; Gies 1987). The origin of runaway stars is still uncertain, but the two leading theories, asymmetric supernovae ejection and dynamical interaction require the existence of a companion (Blaauw 1993, 1961). With more than 30 O stars listed in Table 5, and a binary fraction of at least 50% among the early type stars (Garcia & Mermilliod 2001; Gies 1987), one might expect to see 2 – 3 OB runaways in Cyg OB2. Runaways are usually defined as having space velocities exceeding $30 - 40 \text{ km s}^{-1}$ (Blaauw 1961) relative to their parent cluster or mean local Galactic rotation velocity. Even at minimal runaway speeds, the Association crossing time is $\leq 0.5 \text{ Myr}$ for a diameter of $\sim 30 \text{ pc}$. Thus, any runaways with velocities which are primarily tangential to the line of sight would travel well beyond the canonical boundaries of Cyg OB2 within its lifetime. Comerón et al. (1998) speculates that some of the OB stars in the Cygnus region that have high proper motions may have been ejected from Cyg OB2. Most Cyg OB2 members lack proper motion measurements, and our data are sensitive only to motions in the radial direction. Therefore, we would expect, at most, 1 – 2 runaway stars with large radial velocity components detectable in this survey.

Figure 23 shows that no stars have radial velocities larger than 35 km s^{-1} relative to the mean systemic velocity of the Association. The most notable outliers, which have relative velocities of $20 - 30 \text{ km s}^{-1}$, are also those with the fewest measurements and, therefore, are the most uncertain. We detect no strong candidates for runaway stars. Therefore, we conclude that there is little or no evidence for OB runaways in the radial direction and likely very few runaways within a $\sim 30'$ radius of the cluster center.

6. Conclusions

We conducted a radial velocity survey of the Cygnus OB2 Association over a 6-year time interval to search for MCBs using spectroscopic data from the Keck, Lick, WIYN, and WIRO Observatories. We obtained 1139 spectra to measure radial velocities and radial velocity variations on 146 OB stars. There were 73 identified as new early types. The calculated mean distance modulus for Cyg OB2 stars is $\sim 11.3 \text{ mag}$, which is in good agreement with previous

estimates. Of the 146 total OB stars, analysis of the 143 provisional members yielded an IMF slope of $\Gamma = -2.2 \pm 0.1$. There were a number of minor spectral classification differences, including Cygnus OB2 No. 12 and No. 21. No. 12 showed evidence of a B3Iae spectral classification in at least one epoch and a temperature class variation (B3 – B8) over one year. We utilized two methods for determining velocity variations, including Gaussian profile fitting and cross correlation techniques. Both methods yielded similar results, where 36 stars had a probability $P(\chi^2, \nu) \leq 0.01$ and 9 stars had a probability of $0.01 < P(\chi^2, \nu) \leq 0.04$. In addition, we detected 5 SB2 systems and 8 possible SB2 systems (3 of which were also designated SB1). This translates to a lower limit on the massive binary frequency of 30%(36 out of 120 stars) to 42%(50 out of 120 stars). The calculated velocity dispersion for Cygnus OB2 is $2.44 \pm 0.07 \text{ km s}^{-1}$, which is typical of open clusters, and despite the richness of the association and the number of stars surveyed, we detected no obvious OB runaways.

We thank the time allocation committees of the Lick, Keck, WIYN, and WIRO Observatories for granting us observing time and making this project possible. This paper has been greatly improved by the detailed review and suggestions from an anonymous referee. We are grateful for support from the National Science Foundation through the Research Experiences for Undergraduates (REU) program grant AST-0353760 and through grant AST-0307778, and the support of the Wyoming NASA Space Grant Consortium. The work of C.F. was in part under the auspices of the U.S. Dept. of Energy, and supported by its contract W-7405-ENG-36 to Los Alamos National Laboratory and by National Science Foundation under Grant No. PHY99-07949.

Facilities: WIRO (), WIYN (), Shane (), Keck:I ()

REFERENCES

- Abbott, D. C., Bieging, J. H., and Churchwell, E. 1981, ApJ, 250, 645
- Bate, M. R., & Bonnell, I. A. 1995, MNRAS, 356, 1201
- Bieging, J. H., Abbott, D. C., & Churchwell, E. 1989, ApJ, 340, 518
- Benaglia, P., Romero, G. E., Stevens, I. R., & Torres, D. F. 2001, A&A, 366, 605
- Blaauw, A. 1961, BAN, 15, 265
- Blaauw, A. 1993, IAJ, 16, 141
- Bohannon, B., & Conti, P. S. 1976, ApJ, 204, 797

- Bonnell, I. A., Bate, M. R., & Zinnecker, H. 1998, MNRAS, 298, 93
- de Bruijne, J. H. 1999, MNRAS, 310, 585
- Comerón, F., et al 2002, A&A, 389, 874
- Comerón, F., Torra, J., & Gomez, A. E. 1998, A&A, 330, 975
- Cowley, C., Wiese, W. L., Fuhr, J., & Kuznetsova, L. A. 2000, in *Astrophysical Quantities*, ed. A. N. Cox (4th ed.; New York; Springer), 53
- De Becker, M., Rauw, G., & Manfroid, J. 2004, A&A, 424, L39
- Dequennoy, A., & Mayor, M. 1991, A&A, 248, 485
- Drilling, J. S., & Landolt, A. U. 2000, in *Astrophysical Quantities*, ed. A. N. Cox (4th ed.; New York; Springer), 381
- Fryer, C. L., Burrows, A., & Benz, W. 1998, ApJ, 496, 333
- Fryer, C. L., Woosley, S. E., & Hartmann, D. H. 1999, ApJ, 526, 152
- Fullerton, A. W., Gies, D. R., & Bolton, C. T. 1996, ApJS, 103, 475
- Garcia, B., & Mermilliod, J. C. 2001, A&A, 368, 122
- Garmany, C. D., Conti, P. S., & Massey, P. 1980, ApJ, 242, 1063
- Gies, D. R. 1987, ApJS, 64, 545
- Gottlieb, E. W., & Liller, W. 1978, ApJ, 225, 488
- Hall, D. S. 1974, Acta Astron., 24, 69
- Hanson, M. M. 2003, ApJ, 597, 957
- Harnden, F. R., et al. 1979, ApJ, 234, L51
- Hillwig, T. C., Gies, D. R., Baynuolo, W. G., Huang, W., McSwain, M. V., & Wingert, D. W. 2006, ApJ, 639, 1069
- Humphreys, R. M., & McElroy, D. B. 1984, ApJ, 284, 565
- Johnson, H. L. 1968, in *Nebulae and Interstellar Matter*, ed. B. Middlehurst and L. Aller, University of Chicago Press

- Johnson, H. L., & Morgan, W. W. 1954, *ApJ*, 119, 344
- Jones, B. F.; & Walker, M. F. 1988, *AJ*, 95, 1755
- Kaper, L. 1999, *IAUS*, 193, 316
- Kazarovets, E. V., Samus, N. N., & Durlevich, O. V. 2000, *IBVS*, 4870, 1
- Klochova, V. G., & Chentsov, E. L. 2006, *Astro-ph* 0605483
- Knödseder, J. 2000, *A&A*, 360, 539
- Kukarkin, B. V., et al. 1982, *New Catalogue of Suspected Variable Stars* (Moscow: Nauka)
- Kurtz, M. J., Mink, D. J., Wyatt, W. F., Fabricant, D. G., Torres, G., Kriss, G. A., & Tonry, J. L. 1991, in *Astronomical Data Analysis Software and Systems I*, *ASP Conf. Ser.*, Vol. 25, eds. D.M. Worrall, C. Biemesderfer, and J. Barnes, p. 432
- Lanz, T., & Hubeny, I. 2003, *ApJS*, 146, 417
- Leitherer, C., & Wolf, B. 1982, *MitAG*, 55, 55
- Lejeune T., & Schaerer D. 2001, *A&A*, 366, 538
- Lennon, D. J., Dufton, P. L., & Fitzsimmons, A. 1992, *A&AS*, 94, 569
- Leung, K.-C., & Schneider, D. P. 1978, *ApJ*, 224, L565
- Maeder, A., & Meynet, G. 1988, *A&AS*, 76, 411
- Martins, F., Schaerer, D., & Hillier, D. J. 2005, *A&A*, 436, 1049
- Massey, P., & Thompson, A. B. 1991, *AJ*, 101, 1408
- Massey, P., Johnson, K., & DeGioia-Eastwood, K. 1995, *ApJ*, 454, 151
- Nations, H. L., & Pierce, M. J. 2002, *BAAS*, 200, No. 64.07
- Patriarchi, P., Morbidelli, L., Perinotto, M. 2003, *A&A*, 410, 905
- Penrod, G. D. 1986, *PASP*, 98, 35
- Pigulski, A., & Kolaczowski, Z. 1998, *MNRAS*, 298, 753
- Press, W. H., Teukolsky S. A., Vetterling W. T., & Flannery B. P. 1993, *Numerical Recipes*, (1st ed.; New York, NY: Cambridge University Press)

- Rios, L. Y., & DeGioia-Eastwood, K. 2004, BAAS, 205, No. 09.05
- Romano, G. 1969, MmSAI, 40, 375
- Salpeter, E. E. 1955, ApJ, 121, 161
- Schulte, D. H. 1958, AJ, 128, 41
- Setia Gunawan, D. Y. A., de Bruyn, A. Ger, van der Hucht, Karel, A., Williams, & Peredur, A. 2003, ApJS, 149, 123
- Sharpless, S. 1957, PASP, 69, 239
- Skrutski, M. F., et al. 2006, AJ, 131, 1163
- Snow, T., Zukowski, D., & Massey, P. 2002, ApJ, 578, 877
- Souza, S. P., & Lutz, B. L. 1980, ApJ, 235, L87
- Steenbrugge, K. C., de Bruijne, J. H., Hoogerwerf, R., & de Zeeuw, P. T. 2003, A&A, 402, 587
- Torres-Dodgen, A. V., Tapia, M., & Carroll, M. 1991, MNRAS, 249, 1
- Vanbeveren, D. 2004, EAS, 13, 141
- Vanbeveren, D., De Loore, C., & Van Rensbergen, W. 1998b, A&ARv, 9, 63
- Van den Heuvel, E., & Van der Woerd, H. 1984, A&A, 132, 361
- Voelcker, K. 1975, A&AS, 22, 1
- Vogt, S. S., & Penrod, G. D. 1983, ApJ, 275, 661
- Vogt, S. S., et al. 1994, SPIE, 2198, 362V
- Walborn, N. R. 1973, ApJ, 180, L35
- Walborn, N. R. & Fitzpatrick, E. L. 1990, PASP 102, 379
- Waldron, W. L., Corcoran, M. F., Drake, S. A., & Smale, A. P. 1998, ApJS, 118, 217
- Waldron, W. L., Cassinelli, J. P., Miller, N. A., MacFarlane, J. J., & Reiter, J. C. 2004, ApJ, 616, 542
- Wang, J., & Zhu, Z. 2003, ChPhL, 20, 778

Wegner, W. 1994, MNRAS, 270, 229

Yamashita, Y., & Nariari, K. 1977, An Atlas of Representative Stellar Spectra, (Tokyo, University of Tokyo Press)

Zinnecker, H. 2003, IAUS, 212, 80

Table 1. Observing Information

Date	Observatory/Instrument	Spectral coverage	HJD coverage
1999 July 4 – 5	Keck/HIRES	3890 – 6270 Å in 35 orders	2451363 – 2451364
1999 July 21 – 23	Lick/Hamilton	3650 – 7675 Å in 81 orders	2451381 – 2451383
1999 August 21 – 23	Lick/Hamilton	3650 – 7675 Å in 81 orders	2451411 – 2451413
1999 October 14 – 15	Keck/HIRES	3700 – 5250 Å in 29 orders	2451466 – 2451467
2000 July 10 – 11	Lick/Hamilton	3650 – 7675 Å in 81 orders	2451736 – 2451737
2000 September 18 – 19	Keck/HIRES	3700 – 5250 Å in 29 orders	2451805 – 2451806
2001 August 24	WIYN/Hydra	3800 – 4490 Å in order 2	2452146
2001 September 8 – 9	WIYN/Hydra	3800 – 4490 Å in order 2	2452161 – 2452162
2004 November 28 – 30	WIYN/Hydra	3800 – 4490 Å in order 2	2453338 – 2453340
2005 July 18 – 21	WIRO/WIRO-Spec	3800 – 4490 Å in order 1	2453570 – 2453573
2005 July 18 – 20,22	WIRO/WIRO-Spec	3800 – 4490 Å in order 1	2453632 – 2453635
2005 October 13	WIRO/Longslit	4050 – 6050 Å in order 2	2453657

Table 2. Early Type Stars in the Direction of Cyg OB2

Star (MT)	Lit S.C.	Our S.C.	RA (J2000)	Dec (J2000)	A_V	V	M_V	$(B-V)$	$(B-V)_0$	M_{PD} (M_\odot)	M_0 (M_\odot)	DM	Notes	Ph. Activ.	Ref.
(1)	(2)	(3)	(4)	(5)	(6)	(7)	(8)	(9)	(10)	(11)	(12)	(13)	(14)	(15)	(16)
5	O6V	O6V	20 30 39.87	+41 36 50.9	5.8	12.93	-4.92	1.64	-0.30	31.7	31.7	12.0			
20	...	B0V	20 30 51.12	+41 20 21.6	7.3	14.48	-3.80	2.18	-0.26	17.5	17.5	10.9	n		
21	B(2?)	B2II	20 30 50.75	+41 35 06.0	4.4	13.74	-4.80	1.30	-0.18	18.9	20.0	14.1			
42	...	B2V	20 30 59.43	+41 35 59.6	4.4	13.73	-2.50	1.27	-0.21	10.0	10.0	11.7	n		
59	O8.5V	O8V	20 31 10.57	+41 31 53.0	5.3	11.18	-4.34	1.47	-0.28	22.0	22.0	10.2			
70	O9V	O9V	20 31 18.31	+41 21 21.7	7.1	12.99	-4.05	2.10	-0.28	18.0	18.0	10.0			
83	B1I	B1I	20 31 22.03	+41 31 28.0	4.1	10.64	-6.50	1.18	-0.19	24.0	26.0	13.0		Susp	1
97	...	B2V	20 31 30.49	+41 37 15.6	4.3	14.56	-2.50	1.22	-0.21	10.0	10.0	12.7	n		
103	...	B1V	20 31 33.38	+41 22 49.0	6.7	13.81	-3.20	2.00	-0.23	13.8	13.8	10.3	n		
106	...	B3V	20 31 33.59	+41 36 04.3	4.4	14.60	-1.90	1.29	-0.18	7.6	7.6	12.0	n		
108	...	B3IV	20 31 34.12	+41 31 08.0	4.3	14.88	-2.50	1.26	-0.16	7.6	7.6	13.1	n		
129	...	B3V	20 31 41.60	+41 28 20.9	4.6	14.40	-1.90	1.34	-0.18	7.6	7.6	11.7	n		
138	O8.5I	O8I	20 31 45.39	+41 18 26.8	6.9	12.26	-6.30	1.99	-0.30	36.8	39.8	11.6			
145	O9.5V	O9III	20 31 49.65	+41 28 26.8	4.1	11.52	-5.25	1.11	-0.26	23.1	24.6	12.6			
164	...	B3V	20 31 55.28	+41 35 27.8	4.3	15.07	-1.90	1.25	-0.18	7.6	7.6	12.6	n		
169	B1.5V	B2V	20 31 56.27	+41 33 05.3	4.3	13.90	-2.50	1.21	-0.21	10.0	10.0	12.1			
170	...	B(5?)V	20 31 56.23	+41 35 12.3	3.6	15.21	-1.35	1.05	-0.15	5.9	5.9	11.6	n		
174	B2V	B2IV	20 31 56.90	+41 31 48.0	4.3	12.55	-3.10	1.21	-0.21	10.0	10.0	11.3			
179	...	B3V	20 31 59.82	+41 37 14.3	4.9	14.00	-1.90	1.46	-0.18	7.6	7.6	10.9	n		
186	...	B2Ve	20 32 03.01	+41 32 30.7	4.2	14.14	-2.50	1.20	-0.21	10.0	10.0	12.4	n		
187	B1V	B1V	20 32 03.74	+41 25 10.9	5.3	13.24	-3.20	1.52	-0.23	13.8	13.8	11.1			
189	...	B(6?)V	20 32 04.57	+41 27 48.6	3.9	14.77	-1.15	1.17	-0.14	5.4	5.4	10.8	n		
191	...	B3IV	20 32 04.74	+41 28 44.5	3.6	13.81	-2.50	1.04	-0.16	7.6	7.6	12.7	n		
196	...	B6V	20 32 05.59	+41 27 49.6	4.4	14.81	-1.15	1.31	-0.14	5.4	5.4	10.4	n		
200	...	B3V	20 32 06.85	+41 17 56.8	6.5	13.94	-1.90	1.98	-0.18	7.6	7.6	9.4	n		
202	...	B2V	20 32 07.95	+41 22 00.3	4.7	14.40	-2.50	1.35	-0.21	10.0	10.0	12.2	n		
213	B0V	B0V	20 32 13.07	+41 27 24.9	4.2	11.95	-3.80	1.13	-0.26	17.5	17.5	11.5			
215	B1V	B2V	20 32 13.48	+41 27 31.0	3.5	12.97	-2.50	0.96	-0.21	10.0	10.0	11.9			
216	...	B1.5V	20 32 13.75	+41 27 42.0	4.2	13.02	-2.80	1.18	-0.22	11.9	11.9	11.6	n		
217	O7III _f	O7III _f	20 32 13.77	+41 27 12.7	4.4	10.23	-5.54	1.19	-0.29	31.2	33.0	11.3			
220	...	B1V	20 32 14.56	+41 22 33.7	5.3	14.34	-3.20	1.52	-0.23	13.8	13.8	12.2	n		
221	...	B2V	20 32 14.63	+41 27 40.3	4.5	13.62	-2.50	1.30	-0.21	10.0	10.0	11.5	n		
222	...	B3V	20 32 15.03	+41 19 30.8	5.0	14.80	-1.90	1.47	-0.18	7.6	7.6	11.7	n		

Table 2—Continued

Star (MT)	Lit S.C.	Our S.C.	RA (J2000)	Dec (J2000)	A_V	V	M_V	$(B-V)$	$(B-V)_0$	M_{PD} (M_\odot)	M_0 (M_\odot)	DM	Notes	Ph. Activ.	Ref.
(1)	(2)	(3)	(4)	(5)	(6)	(7)	(8)	(9)	(10)	(11)	(12)	(13)	(14)	(15)	(16)
227	O9V	O9V	20 32 16.53	+41 25 36.4	4.6	11.47	-4.05	1.24	-0.28	18.0	18.0	10.9			
234	...	B2V	20 32 19.66	+41 20 39.7	4.5	13.25	-2.50	1.28	-0.21	10.0	10.0	11.2	n		
238	...	B1V	20 32 21.35	+41 18 35.5	6.1	14.91	-3.20	1.80	-0.23	13.8	13.8	12.0	n		
239	...	B4V	20 32 21.76	+41 34 24.6	3.9	14.33	-1.65	1.14	-0.16	6.4	6.4	10.4	n		
241	...	B2V	20 32 22.15	+41 27 41.7	4.0	13.41	-2.50	1.13	-0.21	10.0	10.0	11.8	n		
248	...	B2V	20 32 25.50	+41 24 51.8	4.6	13.36	-2.50	1.31	-0.21	10.0	10.0	11.2			
250	B1V	B2III	20 32 26.10	+41 29 39.0	3.8	12.88	-3.70	1.06	-0.19	14.8	15.0	12.8			
252	...	B1.5III	20 32 26.50	+41 19 13.7	4.9	14.15	-3.90	1.42	-0.20	16.1	16.3	13.1	n		
255	...	B2III	20 32 27.26	+41 21 56.2	4.8	14.71	-3.70	1.42	-0.19	14.8	15.0	13.5	n		
258	O8V	O8V	20 32 27.67	+41 26 21.7	4.5	11.10	-4.34	1.20	-0.28	22.0	22.0	10.9			
259	B1V	B0Ib	20 32 27.76	+41 28 51.9	3.7	11.42	-6.00	1.00	-0.22	25.0	27.0	13.7			
264	...	B2III	20 32 30.72	+41 07 04.1	3.5	12.63	-3.70	0.99	-0.19	14.8	15.0	12.7	n		
268	...	B2.5V	20 32 31.42	+41 30 51.4	4.9	14.38	-2.20	1.43	-0.19	8.8	8.8	11.7	n		
271	...	B4V	20 32 32.34	+41 22 57.6	5.0	14.57	-1.65	1.51	-0.16	6.4	6.4	9.5	n		
273	...	B(5?)V	20 32 32.54	+41 26 46.7	5.2	14.91	-1.35	1.57	-0.15	5.9	5.9	9.7	n		
275	...	B2V	20 32 32.68	+41 27 04.4	3.9	13.47	-2.50	1.10	-0.21	10.0	10.0	12.0	n		
292	B1V	B2V	20 32 37.03	+41 23 05.1	5.2	13.08	-2.50	1.51	-0.21	10.0	10.0	10.4			
295	...	B2V	20 32 37.78	+41 26 15.3	4.3	13.71	-2.50	1.21	-0.21	10.0	10.0	11.9	n		
298	...	B3V	20 32 38.34	+41 28 56.6	4.3	14.43	-1.90	1.25	-0.18	7.6	7.6	12.0	n		
299	O7V	O7V	20 32 38.58	+41 25 13.6	4.4	10.84	-4.63	1.19	-0.29	26.5	26.5	11.0			
300	B(1?)	B1V	20 32 38.87	+41 25 20.8	4.3	13.05	-3.20	1.21	-0.23	13.8	13.8	11.9			
304	B5Iae	B3Iae	20 32 40.88	+41 14 29.3	10.	11.46	-6.30	3.35	-0.13	22.0	23.5	7.4		Susp	1
311	...	B2V	20 32 42.90	+41 20 16.4	4.8	13.87	-2.50	1.39	-0.21	10.0	10.0	11.5	n		
317	O8V	O8V	20 32 45.45	+41 25 37.3	4.6	10.68	-4.34	1.25	-0.28	22.0	22.0	10.4			
322	...	B2.5V	20 32 46.45	+41 24 22.4	4.6	14.91	-2.20	1.33	-0.19	8.8	8.8	12.5	n		
325	...	B1.5III	20 32 46.74	+41 26 15.9	4.7	14.30	-3.90	1.37	-0.20	16.1	16.3	13.4	n		
336	...	B3III	20 32 49.67	+41 25 36.4	4.0	14.13	-3.00	1.17	-0.16	12.2	12.3	13.1	n		
339	O8.5V	O8V	20 32 50.03	+41 23 44.6	4.9	11.60	-4.34	1.35	-0.28	22.0	22.0	11.0			
343	...	B1V	20 32 50.69	+41 15 02.2	6.6	14.44	-3.20	1.98	-0.23	13.8	13.8	11.0	n		
358	B	B3V	20 32 54.35	+41 15 22.1	7.0	14.81	-1.90	2.16	-0.18	7.6	7.6	9.7			
365	...	B1V	20 32 56.66	+41 23 41.0	4.5	13.81	-3.20	1.28	-0.23	13.8	13.8	12.4	n		
372	...	B0V	20 32 58.79	+41 04 29.9	7.3	14.97	-3.80	2.17	-0.26	17.5	17.5	11.4	n		
376	O8V	O8V	20 32 59.17	+41 24 25.7	4.9	11.91	-4.34	1.35	-0.28	22.0	22.0	11.3			

Table 2—Continued

Star (MT)	Lit S.C.	Our S.C.	RA (J2000)	Dec (J2000)	A _V	V	M _V	(B−V)	(B−V) ₀	M _{PD} (M _⊙)	M ₀ (M _⊙)	DM	Notes	Ph. Activ.	Ref.
(1)	(2)	(3)	(4)	(5)	(6)	(7)	(8)	(9)	(10)	(11)	(12)	(13)	(14)	(15)	(16)
378	B0V	B0V	20 32 59.61	+41 15 14.6	7.1	13.49	-3.80	2.10	-0.26	17.5	17.5	10.2			
390	O8V	O8V	20 33 02.94	+41 17 43.3	6.8	12.95	-4.34	1.98	-0.28	22.0	22.0	10.4		Irr	2
395	B1.5V	B1V	20 33 04.42	+41 17 08.9	6.0	14.14	-3.20	1.75	-0.23	13.8	13.8	11.4	n		
400	B	B1V	20 33 05.22	+41 17 51.6	5.6	14.15	-3.20	1.62	-0.23	13.8	13.8	11.8			
403	B2V	B1V	20 33 05.55	+41 43 37.2	5.2	12.94	-3.20	1.49	-0.23	13.8	13.8	10.9			
409	...	B0.5V	20 33 06.62	+41 21 13.3	6.0	14.21	-3.80	1.76	-0.24	15.6	15.6	12.0	n		
417	O4III	O4III	20 33 08.78	+41 13 18.1	7.1	11.55	-5.98	2.04	-0.31	48.8	51.0	10.4			
420	...	O9V	20 33 09.41	+41 12 58.2	6.8	12.84	-4.05	1.97	-0.28	18.0	18.0	10.1	n,b		
421	O9V	O9V	20 33 09.58	+41 13 00.6	6.7	12.86	-4.05	1.96	-0.28	18.0	18.0	10.1	b	EA, $P = 4.161d$	2
425	B0V	B0V	20 33 10.10	+41 13 10.1	6.6	13.62	-3.80	1.94	-0.26	17.5	17.5	10.8			
426	B0V	BOV	20 33 10.34	+41 13 06.4	6.6	14.05	-3.80	1.95	-0.26	17.5	17.5	11.2			
427	...	B4II-B4III	20 33 10.27	+41 23 44.9	4.6	14.97	-4.60	1.39	-0.13	15.3	15.5	10.4	n		
428	...	B1V	20 33 10.46	+41 20 57.6	6.0	14.06	-3.20	1.77	-0.23	13.8	13.8	11.2	n		
429	B0V	B0V	20 33 10.50	+41 22 22.8	5.5	12.98	-3.80	1.56	-0.26	17.5	17.5	11.3		EA; $P = 2.9788d$:	2
431	O5If	O5If	20 33 10.74	+41 15 08.0	6.4	10.96	-6.33	1.81	-0.32	50.9	53.0	10.9		Unk; $P = 1.22/5.6d$	2
435	...	B0V	20 33 11.02	+41 10 31.9	7.4	14.78	-3.80	2.19	-0.26	17.5	17.5	11.2	n		
441	...	B2(III?)	20 33 11.39	+41 17 58.9	5.1	14.38	-3.70	1.52	-0.19	14.8	15.0	12.9	n		
444	...	B5V	20 33 11.81	+41 24 05.8	4.9	14.12	-1.35	1.48	-0.15	5.9	5.9	9.3	n		
448	O6V	O6V	20 33 13.25	+41 13 28.6	7.4	13.61	-4.92	2.15	-0.30	31.7	31.7	11.1		Unk; $P = 3.16d?$	2
453	...	B(5?)V	20 33 13.37	+41 26 39.7	3.9	14.45	-1.35	1.14	-0.15	5.9	5.9	10.5	n		
455	O8V	O8V	20 33 13.67	+41 13 05.7	6.3	12.92	-4.34	1.81	-0.28	22.0	22.0	10.9			
457	O3If	O3If	20 33 14.16	+41 20 21.5	5.4	10.55	-6.35	1.45	-0.34	80.0	100	11.5		Irr	2
459	...	B(5?)	20 33 14.34	+41 19 33.0	5.8	14.67	-1.35	1.79	-0.15	5.9	5.9	8.8	n		
462	O6.5III	O7III-II	20 33 14.84	+41 18 41.4	5.2	10.33	-5.54	1.44	-0.29	31.2	33.0	10.6		Cst	2
465	O5.5I	O5.5I	20 33 15.18	+41 18 50.1	4.9	9.06	-6.33	1.30	-0.32	48.3	50.3	10.5			
467	B1V	B1V	20 33 15.37	+41 29 56.6	5.5	13.43	-3.20	1.59	-0.23	13.8	13.8	11.1			
469	...	B1III	20 33 15.51	+41 27 32.9	4.9	13.65	-4.30	1.41	-0.21	17.5	18.3	13.0	n		
470	O9V	O9V	20 33 15.74	+41 20 17.2	5.2	12.50	-4.05	1.46	-0.28	18.0	18.0	11.3		Cst	2
473	O8.5V	O8.5V	20 33 16.36	+41 19 01.9	5.2	12.02	-4.19	1.45	-0.28	19.8	19.8	11.0		Cst	2
477	...	B(0?)V	20 33 17.40	+41 12 38.7	6.5	14.43	-3.80	1.91	-0.26	17.5	17.5	11.7	n		
480	O7V	O7V	20 33 17.49	+41 17 09.2	5.6	11.88	-4.63	1.59	-0.29	26.5	26.5	10.8		Cst	2
483	O5I	O5III	20 33 18.02	+41 18 31.0	4.6	10.19	-5.84	1.24	-0.30	41.5	43.0	11.4		Cst	2
485	O8V	O8V	20 33 18.08	+41 21 36.6	5.4	12.06	-4.34	1.51	-0.28	22.0	22.0	11.0		Cst	2

Table 2—Continued

Star (MT)	Lit S.C.	Our S.C.	RA (J2000)	Dec (J2000)	A_V	V	M_V	$(B-V)$	$(B-V)_0$	M_{PD} (M_\odot)	M_0 (M_\odot)	DM	Notes	Ph. Activ.	Ref.
(1)	(2)	(3)	(4)	(5)	(6)	(7)	(8)	(9)	(10)	(11)	(12)	(13)	(14)	(15)	(16)
488	Be	B1Ve-B3Ve	20 33 18.55	+41 15 35.4	7.7	14.88	-3.20	2.36	-0.21	10.0	10.0	10.3		BE	2
490	...	B(0?)	20 33 18.56	+41 24 49.3	5.4	14.76	-3.80	1.53	-0.26	17.5	17.5	13.1	n		
492	...	B1V	20 33 19.16	+41 17 44.9	5.7	14.85	-3.20	1.68	-0.23	13.8	13.8	12.3	n		
493	...	B5IV	20 33 19.26	+41 24 44.8	5.3	14.99	-1.35	1.61	-0.15	5.9	5.9	9.7	n		
507	O9V	O9V	20 33 21.04	+41 17 40.1	5.5	12.70	-4.05	1.54	-0.28	18.0	18.0	11.2		Cst	2
509	...	B0III-B0IV	20 33 21.14	+41 35 52.0	6.1	14.72	-5.00	1.79	-0.23	20.0	20.8	13.6	n		
513	...	B2V	20 33 22.49	+41 22 16.9	4.9	14.26	-2.50	1.42	-0.21	10.0	10.0	11.8	n		
515	B1V	B1V	20 33 23.24	+41 13 41.9	6.8	14.66	-3.20	2.03	-0.23	13.8	13.8	11.0			
516	O5.5V	O5.5V	20 33 23.46	+41 09 12.9	7.5	11.84	-5.07	2.20	-0.30	34.2	34.2	9.5			
517	...	B1V	20 33 23.37	+41 20 17.2	5.2	13.74	-3.20	1.50	-0.23	13.8	13.8	11.7	n		
522	...	B2V(e?)	20 33 24.78	+41 22 04.5	4.8	14.06	-2.50	1.38	-0.21	10.0	10.0	11.7	n	BCEP; $P = 0.21210d?$	2
531	O8.5V	O8.5V	20 33 29.42	+41 21 54.1	5.6	11.58	-4.19	1.57	-0.28	19.8	19.8	10.2			
534	O7.5V	O8.5V	20 33 26.77	+41 10 59.5	6.5	13.00	-4.19	1.87	-0.28	19.8	19.8	10.7			
539	...	B(5?)Ve	20 33 27.21	+41 35 57.8	7.3	14.61	-1.35	2.29	-0.15	5.9	5.9	7.3	n		
554	...	B4Ve	20 33 30.55	+41 20 17.3	4.7	14.41	-1.65	1.41	-0.16	6.4	6.4	9.7	n	EA	2
555	O8V/	...	20 33 30.43	+41 35 57.5	6.6	12.51	-4.34	1.90	-0.28	22.0	22.0	10.2			
556	B1I	B1I	20 33 30.81	+41 15 22.7	5.9	11.01	-6.50	1.77	-0.19	24.0	26.0	11.6		Irr	2
561	...	B2V	20 33 31.68	+41 21 46.1	4.5	13.73	-2.50	1.30	-0.21	10.0	10.0	11.7	n		
568	...	B3V	20 33 33.38	+41 08 36.3	7.0	14.76	-1.90	2.16	-0.18	7.6	7.6	9.6	n		
573	...	B3I	20 33 33.97	+41 19 38.4	5.3	13.87	-6.30	1.62	-0.13	22.0	23.5	14.9	n		
575	B2V	B2Ve	20 33 34.36	+41 18 11.6	5.9	13.41	-2.50	1.77	-0.21	10.0	10.0	9.9			
576	...	B(7?)V	20 33 34.60	+41 21 37.4	4.6	14.71	-1.00	1.39	-0.13	4.6	4.6	10.1	n		
588	B0V	B0V	20 33 37.02	+41 16 11.4	5.8	12.40	-3.80	1.66	-0.26	17.5	17.5	10.4		Cst	2
601	O9.5III	B0Iab	20 33 39.14	+41 19 26.1	5.1	11.07	-6.50	1.47	-0.22	25.0	27.0	12.5		IS:	3
605	B1V	B1V	20 33 39.84	+41 22 52.4	4.3	11.78	-3.20	1.19	-0.23	13.8	13.8	10.7			
611	O7V	O7V	20 33 40.88	+41 30 18.5	5.5	12.77	-4.63	1.55	-0.29	26.5	26.5	11.8			
620	...	B0V	20 33 42.38	+41 11 45.8	6.2	13.89	-3.80	1.82	-0.26	17.5	17.5	11.4	n		
621	...	B1(V?)	20 33 42.57	+41 14 56.9	6.3	14.93	-3.20	1.91	-0.18	13.8	13.8	11.8	n		
632	O9I	O9I	20 33 46.15	+41 33 00.5	5.6	9.88	-6.29	1.59	-0.27	32.0	34.5	10.5			
635	...	B1III	20 33 46.85	+41 08 01.9	5.8	13.81	-4.30	1.72	-0.21	17.5	18.3	12.3	n		
639	...	B2V	20 33 47.63	+41 09 06.5	6.0	14.37	-2.50	1.77	-0.21	10.0	10.0	10.9	n		
641	...	B5(V?)	20 33 47.58	+41 29 57.7	5.0	14.27	-1.35	1.51	-0.15	5.9	5.9	9.3	n		
642	B1III	B1III	20 33 47.88	+41 20 41.7	5.3	11.78	-4.30	1.55	-0.21	17.5	18.3	10.8			

Table 2—Continued

Star (MT)	Lit S.C.	Our S.C.	RA (J2000)	Dec (J2000)	A_V	V	M_V	$(B-V)$	$(B-V)_0$	M_{PD} (M_\odot)	M_0 (M_\odot)	DM	Notes	Ph. Activ.	Ref.
(1)	(2)	(3)	(4)	(5)	(6)	(7)	(8)	(9)	(10)	(11)	(12)	(13)	(14)	(15)	(16)
645	...	B2III	20 33 48.40	+41 13 14.1	6.2	14.65	-3.70	1.87	-0.19	14.8	15.0	12.1	n		
646	B(1.5?)V	B1.5V	20 33 48.88	+41 19 40.9	4.8	13.34	-2.80	1.39	-0.22	11.9	11.9	11.3			
650	...	B2V(e?)	20 33 48.83	+41 37 39.7	5.2	14.94	-2.50	1.53	-0.21	10.0	10.0	12.2	n		
692	B0V	B0V	20 33 59.32	+41 05 38.4	5.9	13.61	-3.80	1.69	-0.26	17.5	17.5	11.5			
696	O9.5V	O9.5V	20 33 59.57	+41 17 36.1	5.8	12.32	-3.90	1.65	-0.27	16.5	16.5	10.4		EW/KE; $P = 1.46d$	4
712	...	B1V	20 34 04.43	+41 08 08.4	6.1	13.66	-3.20	1.80	-0.23	13.8	13.8	10.7	n		
716	O9V	O9V	20 34 04.95	+41 05 13.2	6.4	13.50	-4.05	1.84	-0.28	18.0	18.0	11.1			
720	B?	O9.5V	20 34 06.10	+41 08 09.6	7.0	13.59	-3.90	2.05	-0.27	16.5	16.5	10.5			
734	O5I	O5I	20 34 08.54	+41 36 59.3	5.4	10.03	-6.33	1.49	-0.32	50.9	53.0	10.9		Susp	1
736	O9V	O9V	20 34 09.52	+41 34 13.4	5.2	12.79	-4.05	1.46	-0.28	18.0	18.0	11.6			
745	O7V	O7V	20 34 13.50	+41 35 02.6	5.4	11.91	-4.63	1.50	-0.29	26.5	26.5	11.1			
759	...	B1V	20 34 24.56	+41 26 24.7	5.7	14.65	-3.20	1.67	-0.23	13.8	13.8	12.1	n		
771	O7V	O7V	20 34 29.52	+41 31 45.5	7.0	12.06	-4.63	2.05	-0.29	26.5	26.5	9.6			
793	B1.5III	B2IIIe	20 34 43.51	+41 29 04.8	5.2	12.29	-3.70	1.54	-0.19	14.8	15.0	10.7			

Note. — 1. Star name in MT91 nomenclature; 2. Spectral type obtained from the literature; 3. Spectral type as determined by this survey; 4. Right Ascension, (J2000); 5. Declination (J2000); 6. Calculated visual extinction in magnitudes using MT91 colors, Wegner (1994) intrinsic colors, and $R_V = 3.0$; 7. Apparent magnitude as measured by MT91; 8. Absolute magnitudes from Humphreys & McElroy (1984) (B stars) and Martins et al. (2005) (O stars); 9. Measured colors from MT91; 10. Intrinsic colors from Wegner (1994); 11. Initial masses interpolated from the stellar evolutionary models of Lejeune & Schaerer (2001); 12. Current masses from Martins et al. (2005) and Drilling & Landolt (2000); 13. True distance moduli; 14. Notes: An 'n' denotes new early type classification. A 'b' indicates a close visual double, unresolved in our data; 15. Photometric activity as found in the literature; 16. Literature reference for photometric activity.

References. — (1) Kukarkin et al. (1981); (2) Pigulski & Kolaczowski (1998); (3) Romano (1969); (4) Rios & DeGioia-Eastwood (2004)

Table 3. Non OB Stars

Star (MT)	RA (J2000)	Dec (J2000)	V	S.C.
(1)	(2)	(3)	(4)	(5)
34	20 30 54.41	+41 32 49.3	15.44	G?
35	20 30 54.94	+41 35 45.6	15.63	G-K
50	20 31 05.61	+41 34 30.7	14.33	G
52	20 31 08.25	+41 35 32.3	10.98	F
54	20 31 08.33	+41 35 37.1	11.26	G
62	20 31 11.79	+41 34 24.5	14.76	G
100	20 31 32.44	+41 37 41.3	15.60	G
107	20 31 34.05	+41 31 02.6	14.80	G?
118	20 31 38.59	+41 19 53.8	14.29	F?
126	20 31 41.49	+41 23 03.7	15.02	G
133	20 31 42.68	+41 29 54.5	15.04	G?
137	20 31 44.89	+41 21 38.1	14.47	G
141	20 31 45.91	+41 34 49.2	15.36	G
156	20 31 52.64	+41 25 35.8	15.37	G
235	20 32 19.81	+41 23 51.5	13.99	G
242	20 32 23.57	+41 19 24.3	15.36	G
244	20 32 23.83	+41 19 36.2	15.08	A
267	20 32 31.45	+41 14 08.8	12.87	G
272	20 32 32.39	+41 32 37.3	15.01	G
279	20 32 34.33	+41 04 26.0	13.85	A
289	20 32 35.79	+41 35 37.8	14.71	A
308	20 32 41.37	+41 30 26.7	15.12	G
398	20 33 04.40	+41 32 55.8	14.70	G
430	20 33 10.76	+41 07 20.5	14.41	G
436	20 33 11.07	+41 14 45.6	16.08	K
438	20 33 10.69	+41 39 52.9	14.75	K
463	20 33 14.86	+41 19 34.7	15.01	F
519	20 33 23.85	+41 30 37.8	15.06	G
524	20 33 24.70	+41 40 59.3	13.06	A
526	20 33 25.37	+41 30 28.1	14.59	M
617	20 33 42.15	+41 22 22.8	14.93	late?
637	20 33 46.58	+41 38 34.3	15.00	G
665	20 33 53.65	+41 25 32.3	14.76	K
728	20 34 06.64	+41 43 13.3	15.15	K
735	20 34 09.47	+41 29 43.9	15.38	F
737	20 34 09.85	+41 25 57.5	14.74	G
789	20 34 39.49	+41 37 46.2	11.63	late

Note. — 1. Star name in MT91 nomenclature; 2. Right Ascension (J2000); 3. Declination (J2000); 4. Apparent magnitude as measured by MT91; 5. Spectral type.

Table 4. Complete Table of Observations and Radial Velocities

Star (MT)	HJD	Rad. Vel. (km s ⁻¹)	σ_v (km s ⁻¹)
(1)	(2)	(3)	(4)
020	2451365.033	-10.9	4.5
020	2451467.752	-11.7	3.9
020	2451805.998	-18.5	4.5
...

Note. — 1. Star name in MT91 nomenclature; 2. Heliocentric Julian date; 3. Heliocentric radial velocity; 4. 1σ uncertainty. The full contents of Table 4 are available in machine-readable form in the electronic edition of the *Astrophysical Journal*.

Table 5. Derived Radial Velocity Parameters

Star (MT)	S.C.	N _{obs}	V _{avg} (km s ⁻¹)	V _{mid} (km s ⁻¹)	V _h (km s ⁻¹)	V _{rms} (km s ⁻¹)	$\bar{\sigma}_v$ (km s ⁻¹)	P(χ^2, ν)	Sp. Activ.
(1)	(2)	(3)	(4)	(5)	(6)	(7)	(8)	(9)	(10)
20	B0V	8	-13.1	-22.2	12.2	9.1	6.9	0.607	
21	B2II	4	-40.8	-38.4	17.6	16.0	7.1	0.000	SB1
59	O8V	17	-10.1	-29.1	77.3	54.1	11.0	0.000	SB1
70	O9V	7	-6.4	-15.1	12.6	8.8	4.9	0.102	
83	B1I	12	-4.7	-4.8	3.7	2.3	1.8	0.000	SB1
97	B2V	7	-4.4	-8.9	16.8	13.3	11.0	0.306	
103	B1V	5	-26.4	-15.9	18.3	14.6	9.8	0.382	
106	B3V	6	-6.2	-9.4	13.7	8.9	7.9	0.111	
129	B3V	6	-12.3	-15.1	13.6	9.7	12.3	0.742	
138	O8I	15	-7.7	19.7	58.2	31.2	8.7	0.000	SB1
145	O9III	18	-12.4	-22.7	41.1	28.4	3.5	0.000	SB1
164	B3V	3	-8.6	-13.7	11.4	11.6	14.0	0.695	
169	B2V	3	-24.5	-27.6	10.5	11.7	7.8	0.179	
174	B2IV	6	-17.5	-16.5	6.6	5.8	3.1	0.001	SB1
187	B1V	5	-5.1	-3.8	3.6	2.8	5.3	0.971	
191	B3IV	7	-10.4	-9.5	5.5	3.7	5.2	0.942	
196	B6V	3	-34.2	-34.5	37.8	41.9	16.2	0.001	SB1
200	B3V	6	-6.1	4.8	15.9	11.6	12.1	0.915	
202	B2V	5	-2.0	15.9	34.4	27.0	13.1	0.000	SB1
213	B0V	10	2.8	11.2	27.8	19.7	13.3	0.215	
215	B2V	3	-2.8	-1.4	3.1	3.3	14.0	0.988	
216	B1.5V	4	-14.7	-13.5	5.4	5.7	7.4	0.785	
217	O7III _f	12	-6.5	-5.9	4.4	2.6	5.0	0.884	
220	B1V	6	-11.2	-6.9	13.2	10.6	7.8	0.073	
227	O9V	14	-8.4	-19.1	30.5	14.9	10.0	0.416	
234	B2V	7	-16.2	-11.8	17.8	12.1	5.2	0.000	SB1
238	B1V	4	-7.5	-4.4	30.6	25.3	14.7	0.029	SB1?
239	B4V	7	2.5	-1.1	13.7	10.1	13.3	0.851	
241	B2V	5	-6.3	-4.7	13.6	10.3	4.8	0.001	SB1
248	B2V	5	-12.7	-22.7	12.8	10.5	9.0	0.456	
250	B2III	5	-8.8	-9.9	3.8	3.0	3.3	0.598	
252	B1.5II	8	-3.7	2.7	32.7	19.5	7.6	0.000	SB1/SB2
255	B2III	7	-12.9	-13.2	10.1	8.2	7.6	0.412	
258	O8V	17	-20.1	2.6	64.0	34.6	10.2	0.000	SB1
259	B0Ib	11	-14.2	-19.0	10.4	5.6	3.5	0.014	SB1?
264	B2III	7	-1.7	-1.7	5.2	3.7	6.6	0.831	
268	B2.5V	7	-26.3	-22.5	28.6	23.6	8.8	0.000	SB1
271	B4V	6	-31.1	-30.3	22.2	16.5	14.9	0.268	
275	B2V	4	-18.6	-19.9	7.5	6.3	8.3	0.879	
292	B2V	7	-12.9	-4.0	22.4	15.8	5.6	0.000	SB1/SB2?
295	B2V	4	-5.2	-5.9	2.4	2.0	6.6	0.992	
298	B3V	7	-23.8	3.0	40.5	31.3	17.8	0.029	SB1?
299	O7V	16	-15.7	-14.2	24.1	12.5	9.9	0.214	
300	B1V	6	-12.7	-11.9	5.7	5.2	4.4	0.207	

Table 5—Continued

Star (MT)	S.C.	N _{obs}	V _{avg} (km s ⁻¹)	V _{mid} (km s ⁻¹)	V _h (km s ⁻¹)	V _{rms} (km s ⁻¹)	$\overline{\sigma}_v$ (km s ⁻¹)	P(χ^2, ν)	Sp. Activ.
(1)	(2)	(3)	(4)	(5)	(6)	(7)	(8)	(9)	(10)
311	B2V	6	12.2	5.9	28.8	22.7	9.0	0.000	SB1
317	O8V	13	-11.64	3.6	19.7	10.9	10.1	0.834	
322	B2.5V	6	-27.3	-21.7	17.1	12.7	11.0	0.512	
325	B1.5II	6	-8.2	-9.0	4.3	3.1	4.4	0.843	
336	B3III	7	-12.8	-12.4	14.4	10.2	5.5	0.001	SB1
339	O8V	13	-15.1	-15.3	24.4	11.8	6.9	0.299	
343	B1V	7	-5.2	-6.5	12.3	10.1	9.6	0.571	
365	B1V	6	-12.1	-12.9	11.5	7.6	7.5	0.759	SB2?
372	B0V	3	-5.7	-3.8	63.2	63.7	11.5	0.000	SB1
376	O8V	11	-14.0	-26.8	19.0	11.2	9.3	0.716	
378	B0V	7	-21.9	-4.9	38.6	25.9	11.1	0.001	SB1/SB2?
390	O8V	6	-16.7	-20.0	11.6	8.3	9.1	0.567	
395	B1V	8	-14.6	-17.4	8.3	5.1	2.8	0.047	
400	B1V	6	-9.8	-9.1	5.3	4.0	5.7	0.775	
403	B1V	8	-7.0	-18.1	41.2	33.9	8.2	0.000	SB1
409	B0.5V	7	-15.5	-11.3	13.9	11.1	10.6	0.428	
428	B1V	7	-2.4	-5.1	12.4	8.5	4.7	0.000	SB1
429	B0V	8	-15.9	8.6	34.7	23.2	5.3	0.000	SB1
431	O5If	13	-16.1	-14.7	48.0	23.4	13.0	0.083	
435	B0V	5	-10.3	-9.9	11.0	8.8	11.2	0.633	
441	B2III?	5	-9.3	-8.1	4.4	3.8	6.1	0.908	
448	O6V	4	-33.0	-5.0	39.3	37.0	13.8	0.003	SB1
453	B5?V	4	0.1	-10.8	15.7	14.2	9.3	0.299	
457	O3If	11	-27.6	-28.1	14.1	8.4	8.2	0.570	
462	O7III	13	-11.3	-2.3	19.4	9.6	7.6	0.452	
465	O5.5I	17	-10.6	-11.5	16.5	9.6	6.5	0.000	SB1/SB2 ^a
467	B1V	5	-10.2	-6.8	13.3	11.5	10.7	0.551	
469	B1III	5	-10.6	-10.5	3.1	2.5	3.3	0.851	
470	O9V	6	-19.8	-30.2	18.1	13.4	7.9	0.226	
473	O8.5V	10	-5.5	-9.4	35.5	22.5	13.3	0.208	
477	B0V	6	-10.2	-13.4	17.1	12.9	17.7	0.753	
480	O7V	11	-12.6	-13.5	21.3	12.0	13.5	0.595	
483	O5III	12	-15.5	-12.6	22.7	11.5	8.2	0.025	SB1?
485	O8V	8	-11.9	-34.7	29.3	18.7	7.8	0.020	SB1?
490	B0?	5	-10.9	5.4	39.7	29.2	19.6	0.112	
492	B1V	4	14.6	23.5	40.8	36.0	14.8	0.000	SB1
493	B5IV	4	-5.1	3.1	57.2	48.7	13.7	0.000	SB1
507	O9V	5	-16.6	-19.5	6.3	5.1	7.1	0.679	
509	B0III	4	-13.4	-11.6	3.3	2.9	4.7	0.964	
513	B2V	5	-11.6	-35.0	36.7	31.3	7.3	0.000	SB1
515	B1V	7	-7.3	-9.6	12.4	7.5	6.5	0.559	
516	O5.5V	11	-8.3	4.7	56.6	26.6	14.1	0.115	
517	B1V	6	-3.4	-5.1	12.0	10.1	5.9	0.014	SB1?
522	B2Ve?	7	0.6	25.1	60.9	41.3	13.5	0.000	SB1

Table 5—Continued

Star (MT)	S.C.	N _{obs}	V _{avg} (km s ⁻¹)	V _{mid} (km s ⁻¹)	V _h (km s ⁻¹)	V _{rms} (km s ⁻¹)	$\bar{\sigma}_v$ (km s ⁻¹)	P(χ^2, ν)	Sp. Activ.
(1)	(2)	(3)	(4)	(5)	(6)	(7)	(8)	(9)	(10)
531	O8.5V	6	-14.8	-17.0	7.9	5.4	4.0	0.171	
534	O8.5V	6	-13.8	-14.6	6.6	4.6	6.4	0.632	
555	O8V	7	-6.5	-9.6	19.4	14.6	7.6	0.002	SB1
556	B1I	14	-6.3	0.2	14.0	7.1	3.7	0.000	SB1
561	B2V	6	-15.4	-19.0	23.8	19.8	6.8	0.000	SB1/SB2?
568	B3V	7	-14.1	-11.2	26.2	19.6	13.2	0.042	
573	B3I	7	-10.7	-9.7	7.6	6.7	5.1	0.010	SB1?
576	B7?V	5	-1.4	-4.5	5.5	4.5	10.3	0.979	
588	B0V	5	-4.9	-16.5	22.1	17.6	9.6	0.062	
601	B0Iab	8	3.0	-2.6	15.6	9.5	5.1	0.000	SB1
605	B1V	11	-11.0	-20.2	26.2	13.8	9.0	0.470	SB2?
611	O7V	5	-22.7	-23.1	1.4	1.2	4.5	0.998	
620	B0V	6	-11.2	-8.6	14.9	10.1	5.7	0.031	SB1?
621	B1V?	5	-4.9	-10.0	16.3	12.1	10.8	0.695	
632	O9I	14	-2.3	-9.8	13.6	6.7	5.6	0.253	
635	B1III	8	-8.2	-14.0	8.5	5.4	2.3	0.111	
639	B2V	4	-3.1	25.2	44.2	40.5	17.8	0.104	SB2?
641	B5V?	7	-13.8	-12.0	12.0	7.1	14.7	0.995	
642	B1III	15	-8.7	-26.1	39.2	20.1	7.7	0.000	SB1
645	B2III	6	-10.1	-7.3	5.4	4.2	4.2	0.233	
646	B1.5V	5	-7.9	-11.3	9.7	7.6	6.1	0.300	
650	B2Ve?	5	-8.6	-16.3	14.6	11.3	12.9	0.792	
692	B0V	6	-4.2	-6.3	10.4	8.3	9.6	0.778	SB2?
696	O9.5V	9	0.4	-6.9	49.7	33.3	16.2	0.000	SB1/SB2 ^b
712	B1V	5	-13.8	-1.7	20.3	16.4	13.6	0.313	
716	O9V	5	-11.5	-14.8	7.9	6.2	4.5	0.351	
720	O9.5V	5	-6.9	-17.2	90.6	67.7	20.3	0.000	SB1/SB2
734	O5I	15	-27.5	-11.8	39.2	23.5	6.7	0.000	SB1
736	O9V	5	-12.3	-13.0	4.0	3.2	6.0	0.909	
745	O7V	12	-15.8	-39.5	50.4	24.7	11.6	0.035	SB1?
759	B1V	6	-14.5	-15.6	6.4	5.3	6.4	0.794	SB2?
771	O7V	10	-8.1	-14.6	69.1	35.0	13.4	0.000	SB1/SB2

Note. — 1. Star name in MT91 nomenclature; 2. Spectral types as determined/accepted by this survey; 3. Number of usable observations; 4. The weighted average heliocentric velocity; 5. $V_{mid} \equiv 0.5(V_{max} + V_{min})$, the simple average of the largest and smallest observed heliocentric velocity; 6. $V_h = 0.5(V_{max} - V_{min})$, a measure of the velocity semi-amplitude; 7. The RMS heliocentric velocity dispersion of all observations; 8. The mean velocity uncertainty, averaged over all observations; 9. The probability (P) that χ^2 would be exceeded by chance, given $\nu = N_{obs} - 1$ degrees of freedom; 10. Spectroscopic activity where “SB1” represents probable single-lined variability ($P(\chi^2, \nu) \leq 0.01$), “SB1” represents possible single-lined variability ($0.01 < P(\chi^2, \nu) \leq 0.04$), “SB2?” represents a possible double-lined binary signature, and “SB2” is a definite double-lined signature.

^aSpectroscopic period of $P = 21.908d$ (De Becker et al. 2004).

^bPhotometric period of $P = 1.46d$ (Rios & DeGioia-Eastwood 2004).

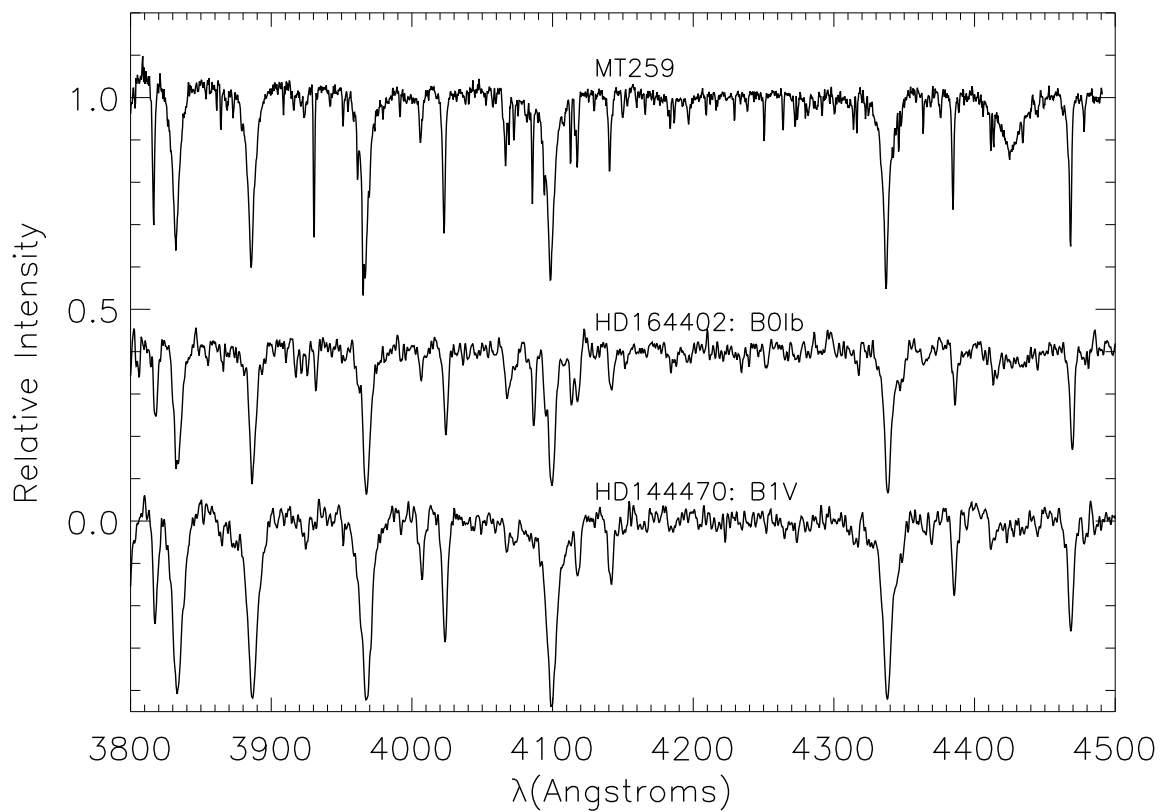


Fig. 1.— 2001 September 9 WIYN spectrum of MT259 (Cyg OB2 No. 21) and comparison spectra from Walborn & Fitzpatrick (1990). MT259 is more consistent with a B0Ib classification.

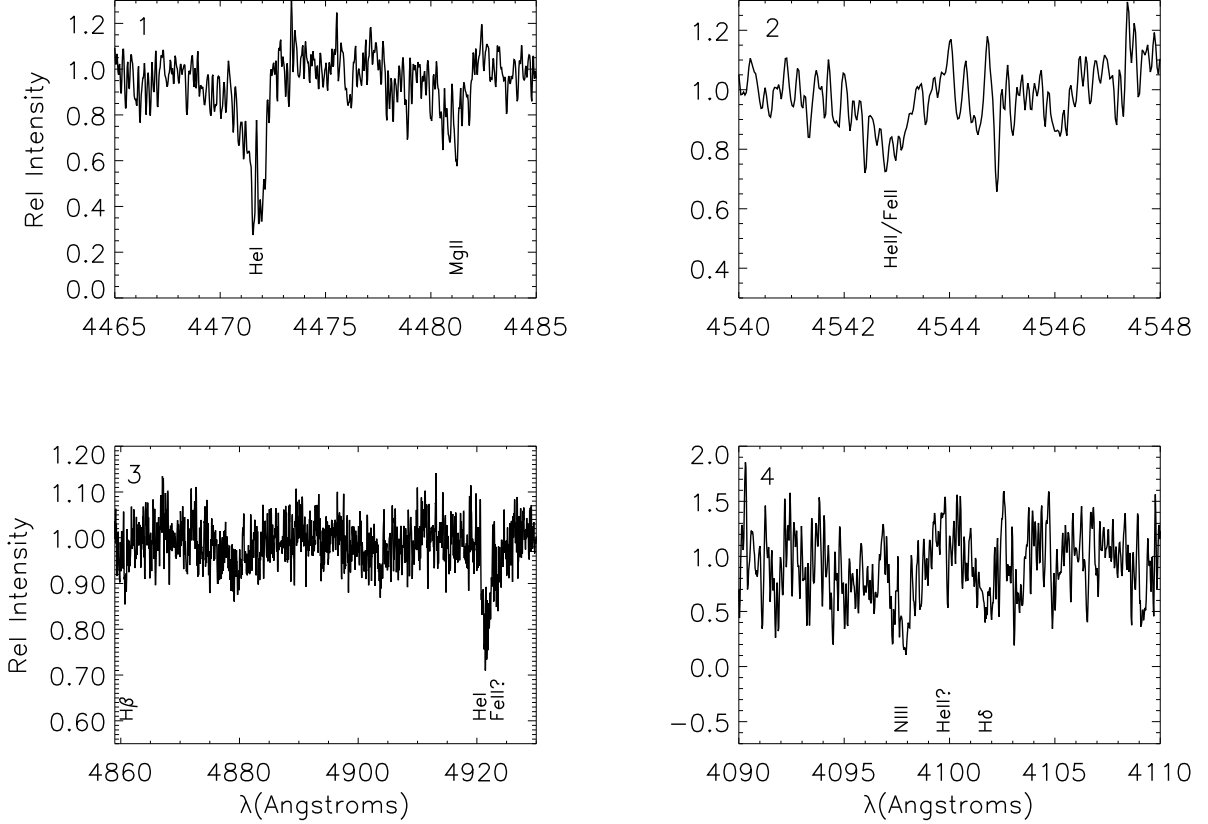


Fig. 2.— A close up of portions of MT304 (Cyg OB2 No. 12) from the 2000 September 18 spectrum taken at Keck. Panel one shows the important He I $\lambda 4471$ to Mg II $\lambda 4481$ Å ratio of approximately 2:1. Panel two shows a He II/Fe II blend at $\lambda 4542$ Å, very weak in early B stars, and absent in later types. Panel three shows He I $\lambda 4922$ Å and an H β line filled in by emission. The strength of $\lambda 4922$ Å and the weak or absent Fe II indicate a type of B5 or earlier. Panel four shows an emission-filled H δ , N III $\lambda 4097$ Å and possible He II $\lambda 4100$ Å.

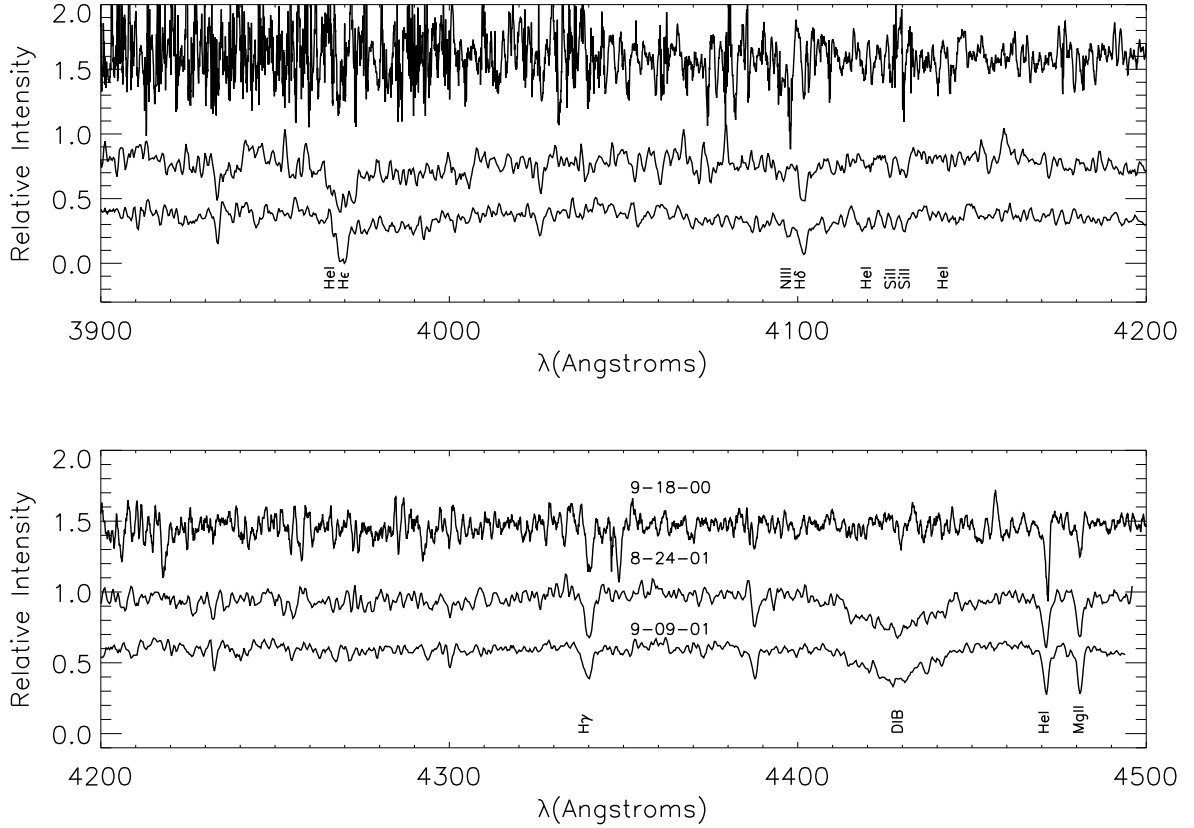


Fig. 3.— A comparison of the spectra for MT304 (Cyg OB2 No. 12) obtained over one year: Keck 2000 September 18 (smoothed by 3 Å) followed by WIYN 2001 August & September. Changes in Balmer line equivalent width, the N III λ 4097 depth, and the He I λ 4471 Å to Mg I λ 4481 Å ratios are also shown. The sequence shows an evolution from B3I in 2000 September to at least B8I in 2001 September.

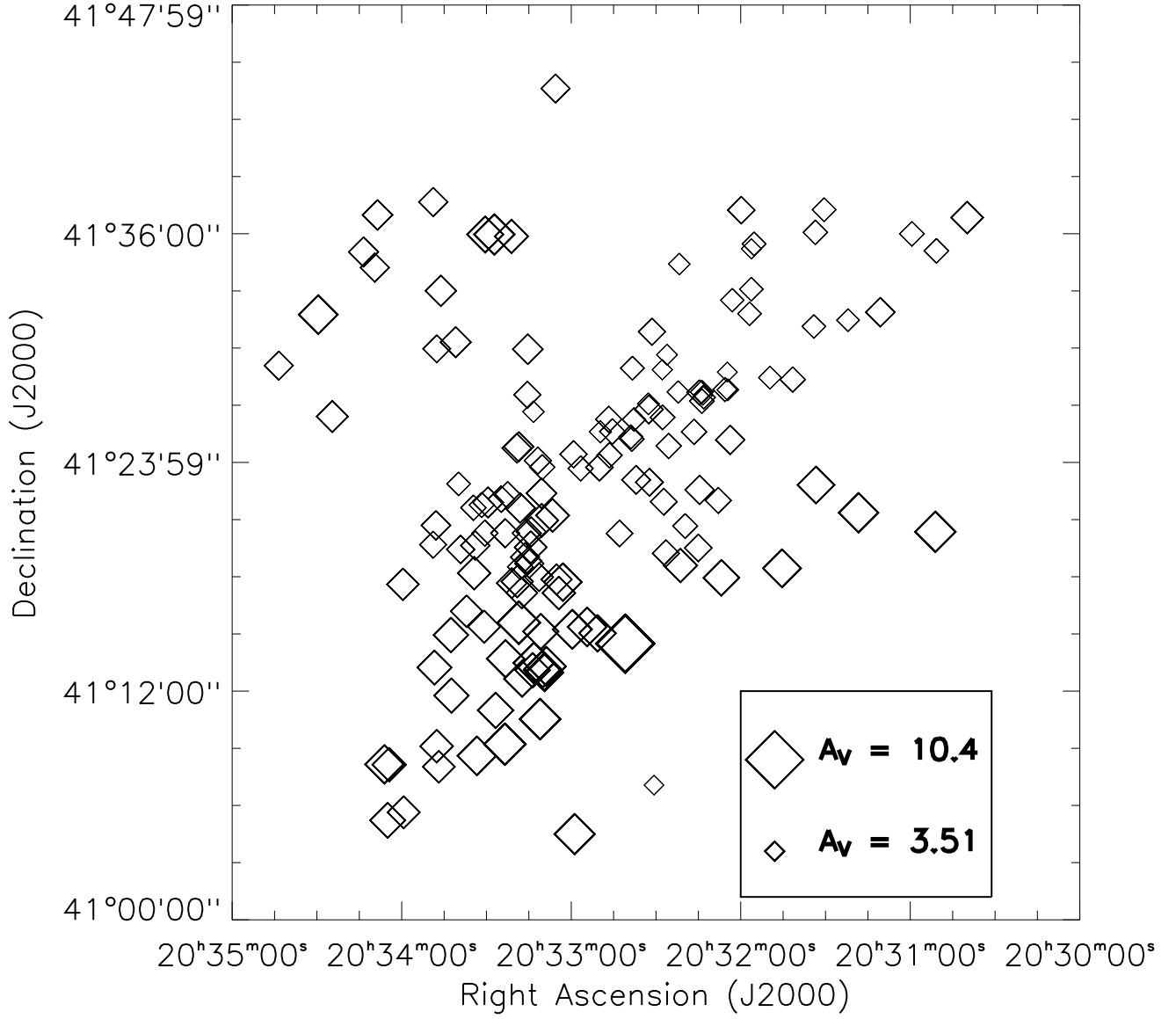


Fig. 4.— A map of calculated extinction, A_V , for 146 OB stars in the direction of Cygnus OB2. The relative size of the symbol is proportional to A_V .

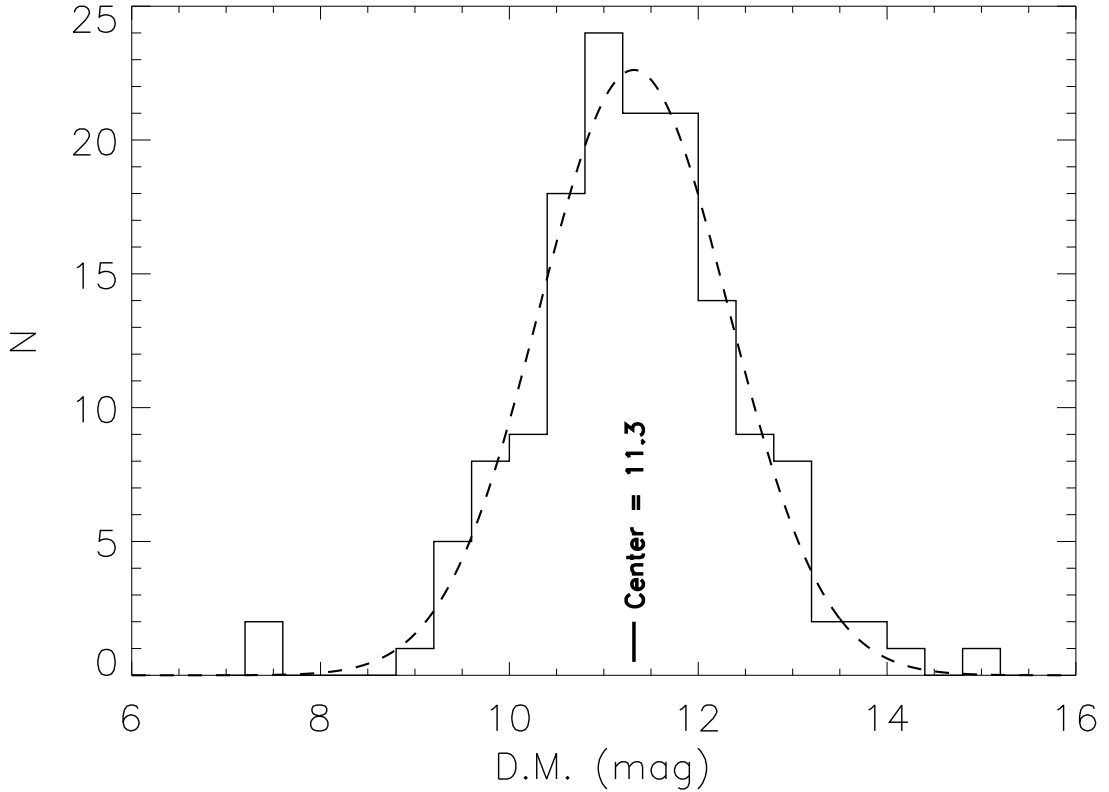


Fig. 5.— Histogram of spectrophotometric distances to the 146 OB stars in the direction of Cygnus OB2. The mean distance modulus is 11.3 magnitudes or ~ 1.8 kpc. The approximately Gaussian dispersion is due to uncertainties in the absolute magnitudes, particularly of the post-main-sequence stars. We adopt all stars with distance moduli between 8.5 and 14.5 as provisional members of the association while acknowledging that this generous range includes some foreground and background objects.

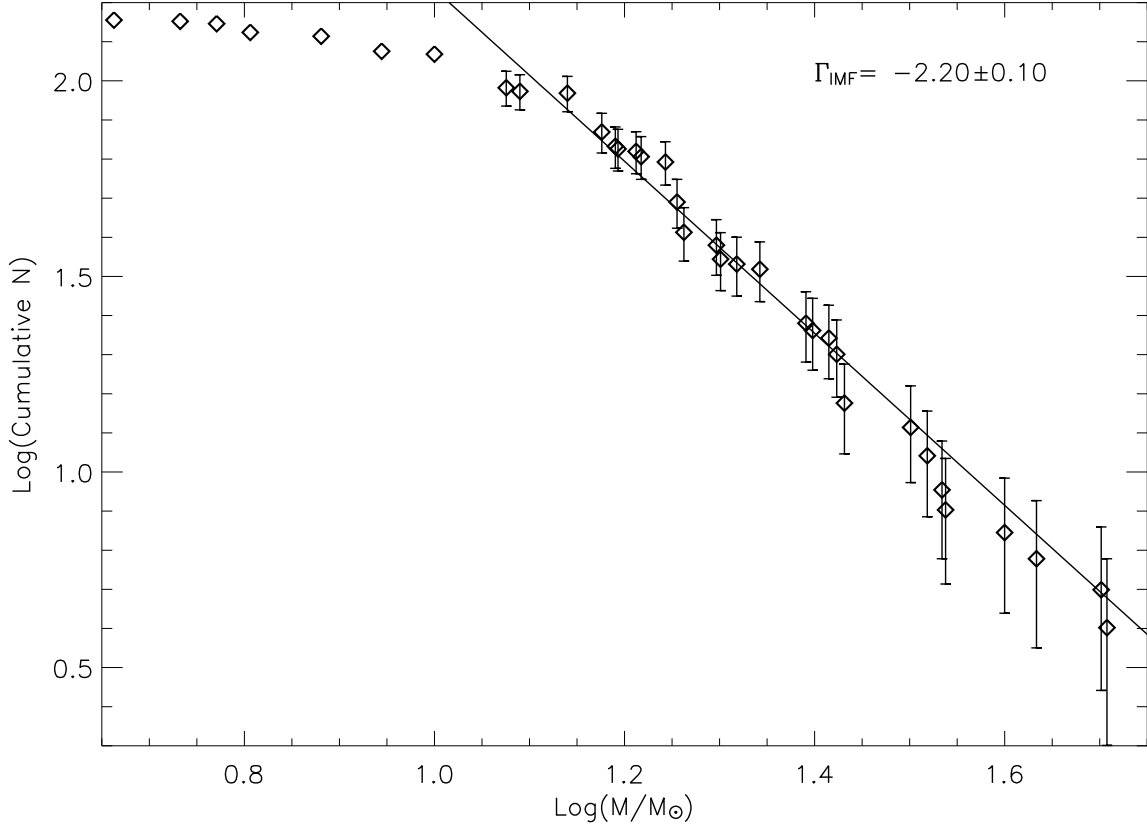


Fig. 6.— A plot of mass distribution for provisional members of Cyg OB2. The initial mass function is calculated using a cumulative mass count. The solid line is a linear fit to masses greater than $\log(M/M_{\odot}) = 1.0$. A slope of $\Gamma = -2.2 \pm 0.1$ has been calculated. Limiting the analysis to stars having distance moduli within 1.5 mag of the mean does not change the slope by more than 0.04.

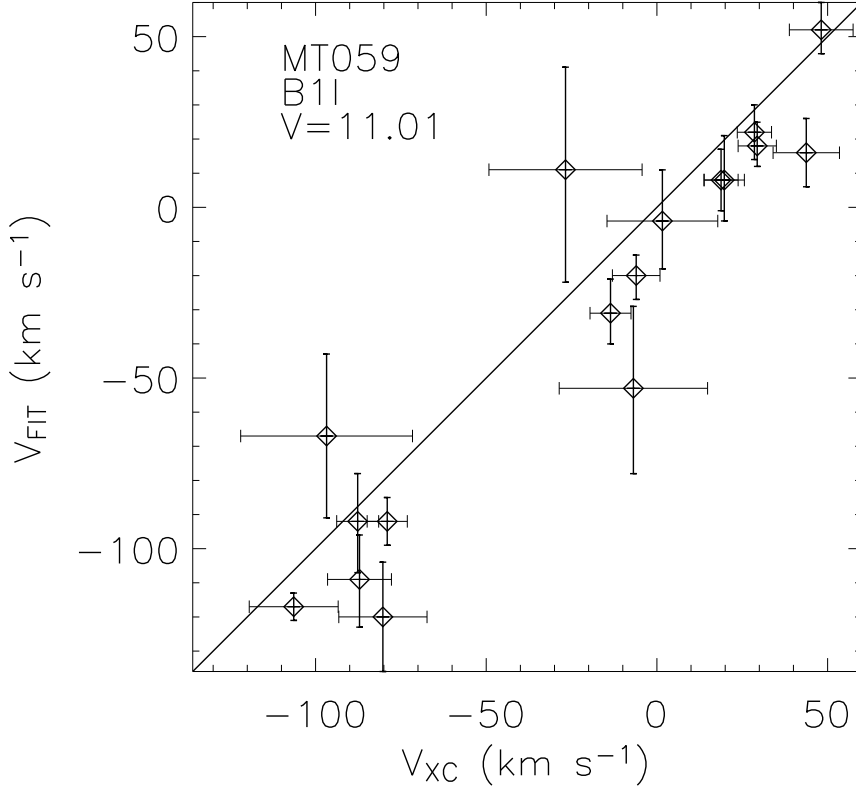


Fig. 7.— A comparison of relative radial velocity results for Gaussian profile fitting versus cross-correlation techniques for MT059. A minor offset of $\sim 10 - 15 \text{ km s}^{-1}$ is observed in most comparisons, most likely attributed to the use of a model atmosphere as a template for the cross-correlation. On average, the larger errors belong to the Gaussian profile fitting.

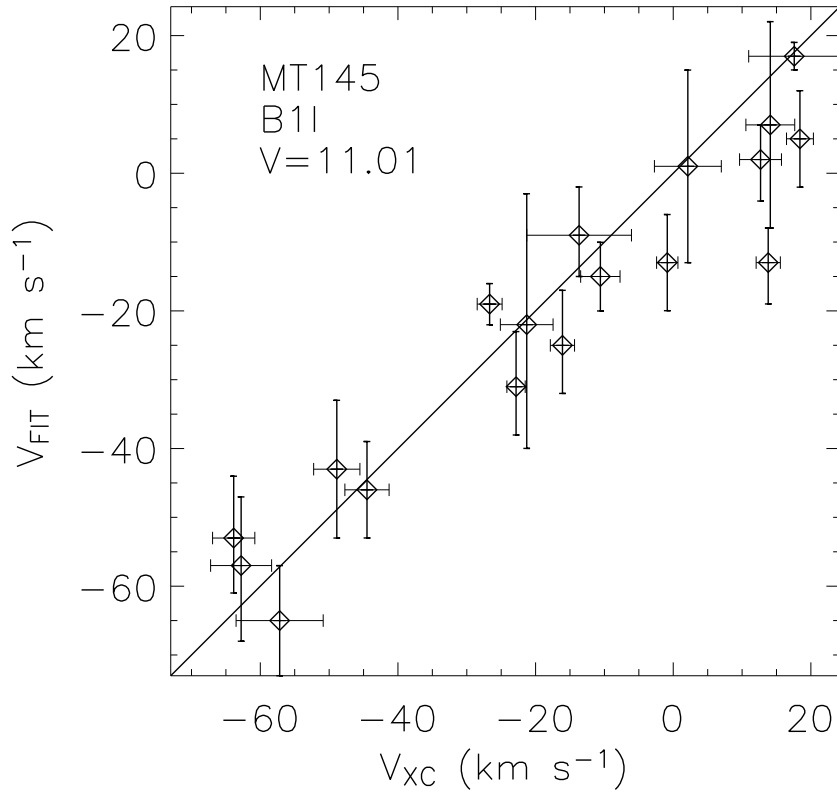


Fig. 8.— A comparison of relative radial velocity results for Gaussian profile fitting and cross-correlation techniques for MT145.

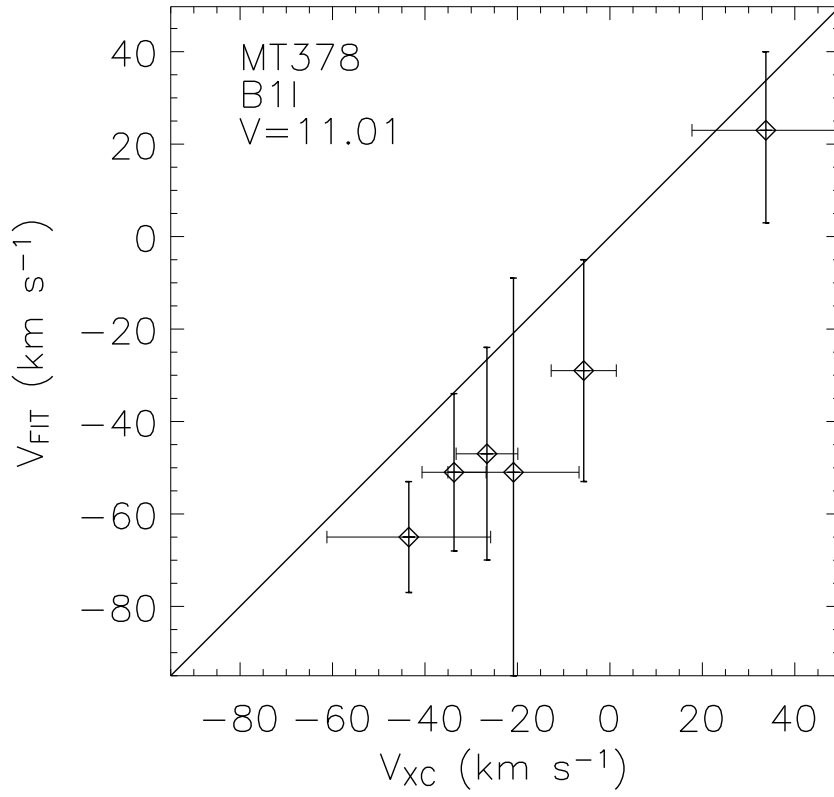


Fig. 9.— A comparison of relative radial velocity results for Gaussian profile fitting and cross-correlation techniques for MT378.

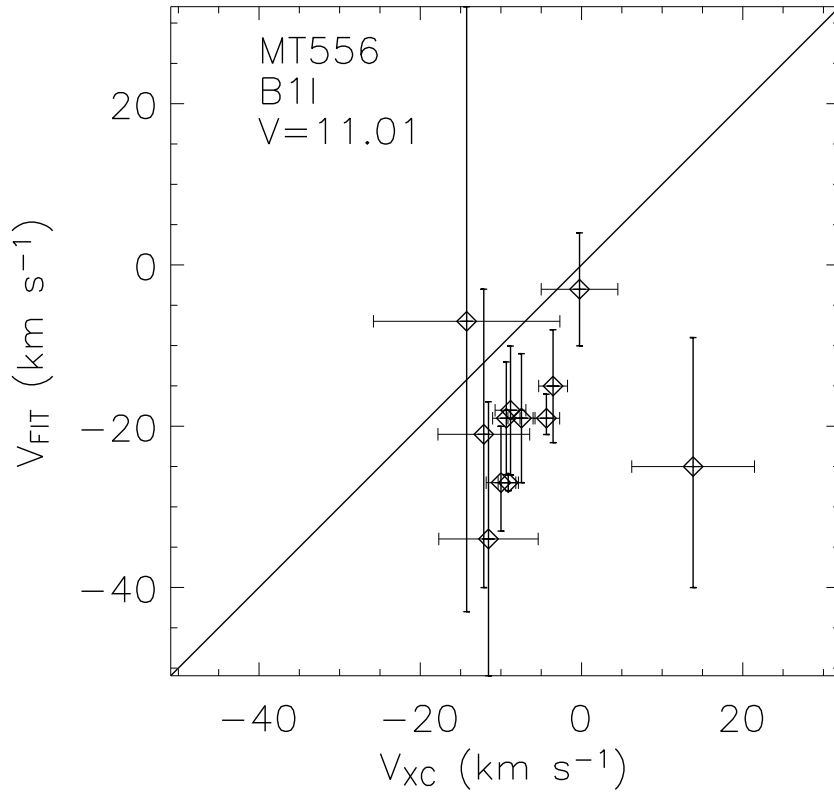


Fig. 10.— A comparison of relative radial velocity results for Gaussian profile fitting and cross-correlation techniques for MT556.

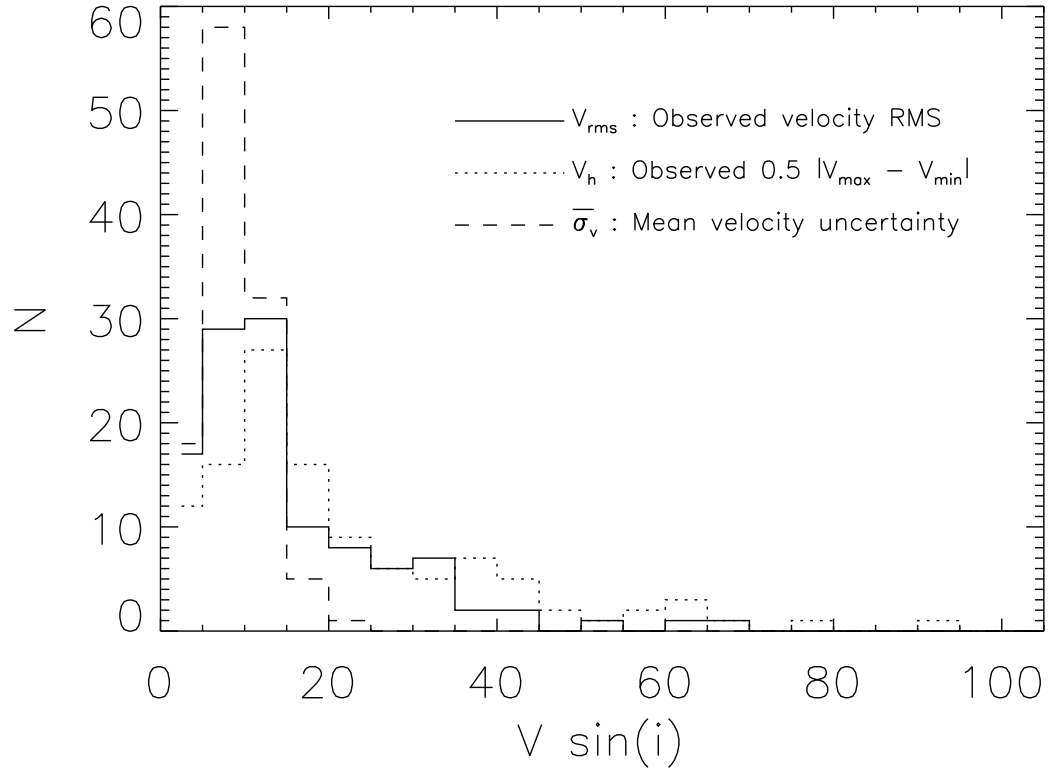


Fig. 11.— The distribution of observed velocity dispersions, V_{rms} (solid line), velocity semi-amplitudes, $V_h \equiv 0.5|V_{max} - V_{min}|$ (dotted line), and the mean velocity uncertainties (dashed line) for the sample.

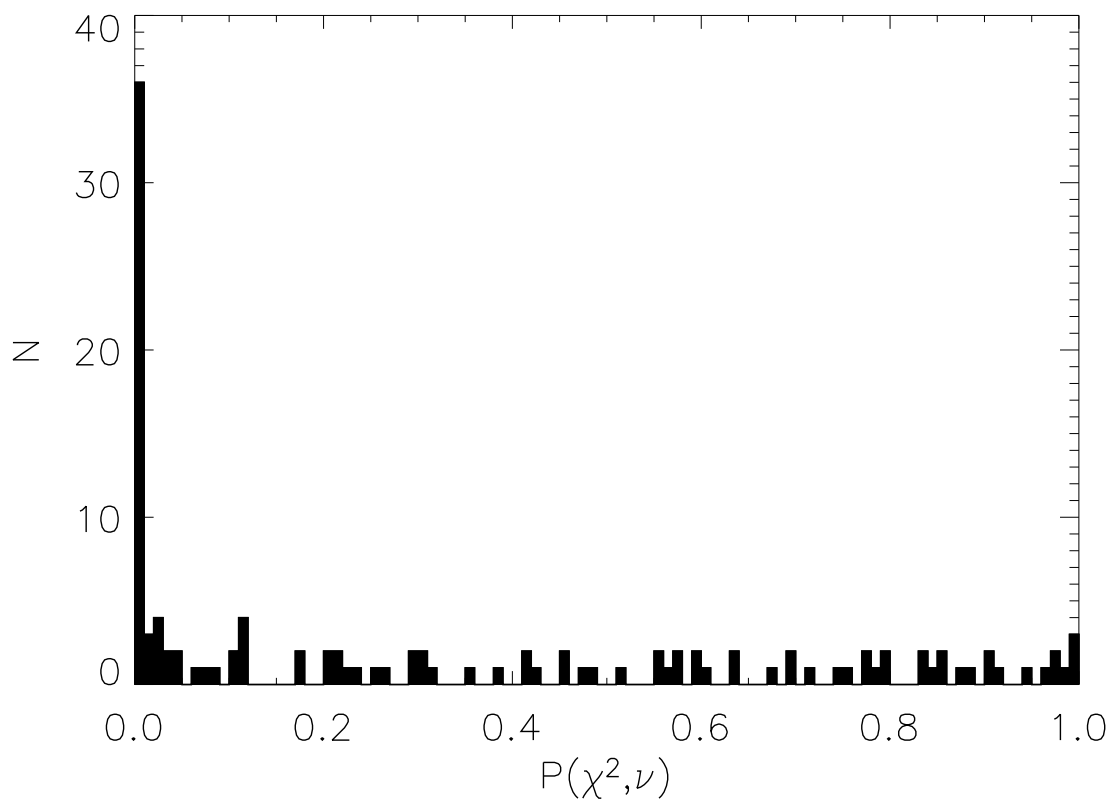


Fig. 12.— The distribution of probabilities that χ^2 (as determined about the weighted mean) would be exceeded given $\nu = N_{obs} - 1$ degrees of freedom. The discontinuity at $P(\chi^2, \nu) = 0.01$ shows the change in the distribution from probable non-variables to probable variables within the sample.

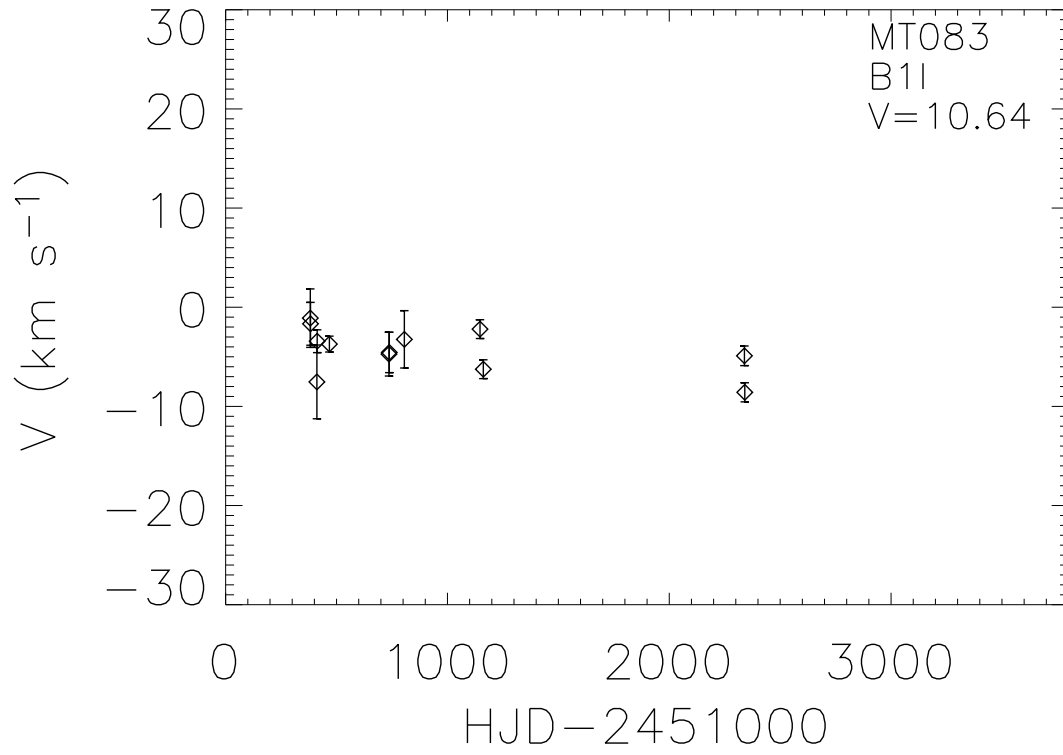


Fig. 13.— Relative radial velocity variation for MT083. MT083 shows variations $\leq 5 \text{ km s}^{-1}$ but is considered an SB1 since $P(\chi^2, \nu) < 0.0004$

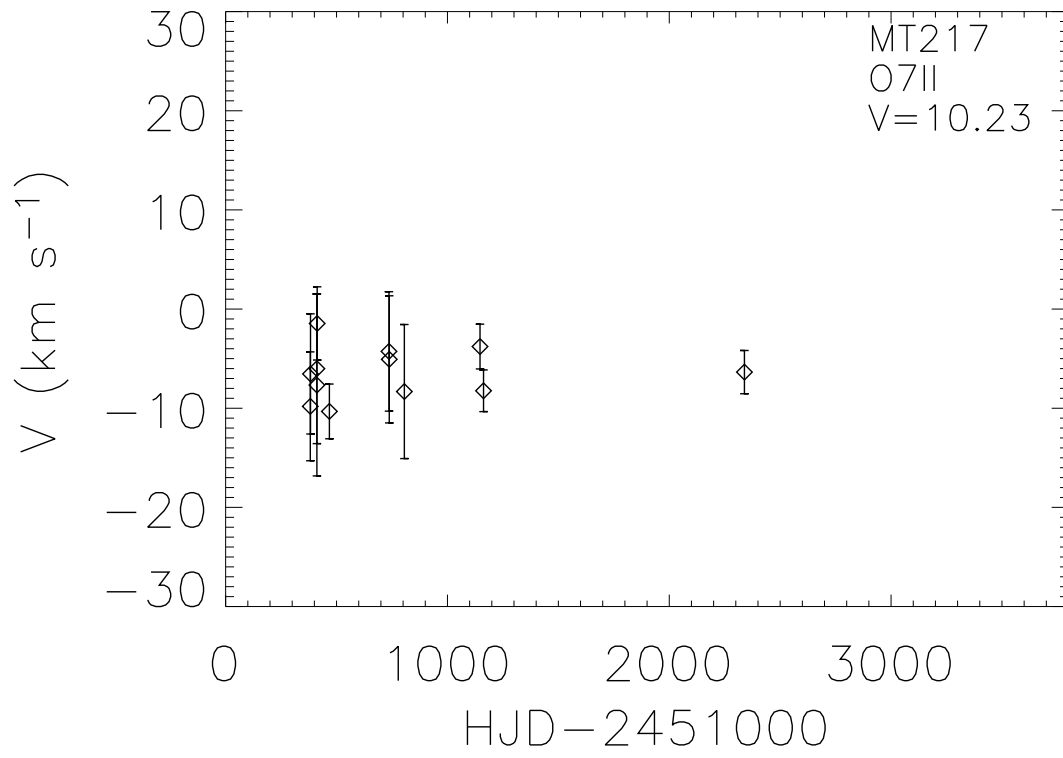


Fig. 14.— Relative radial velocity variation for MT217, a system with little or no variation.

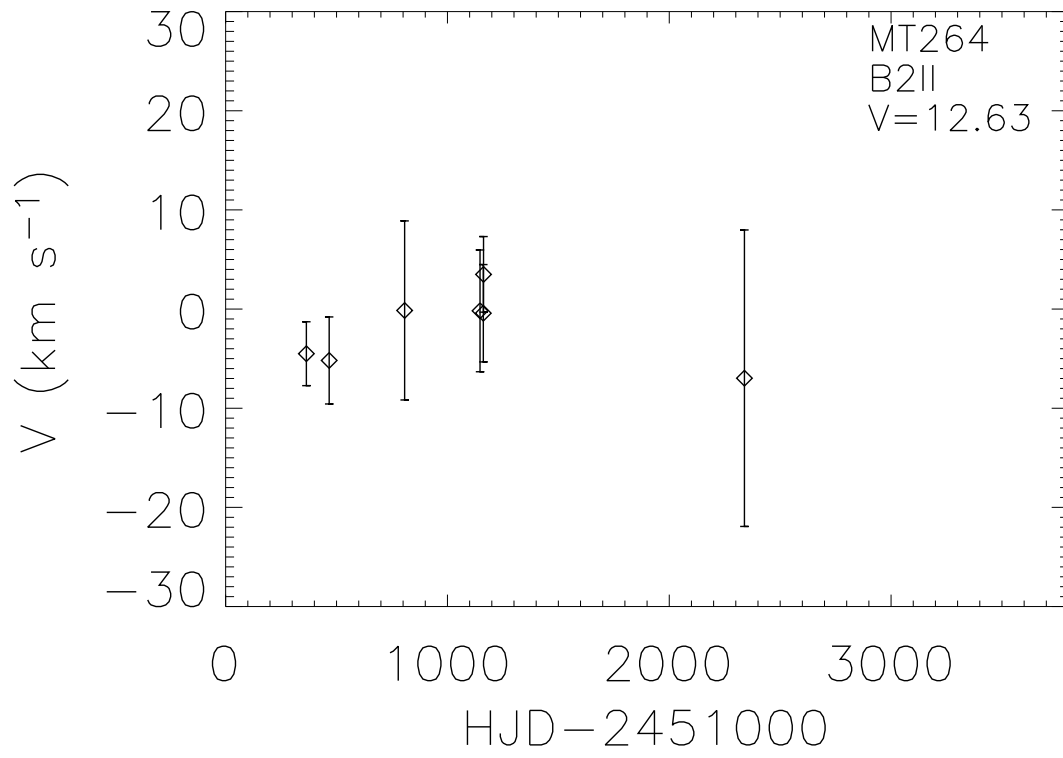


Fig. 15.— Relative radial velocity variation for MT264, a system with little or no variation.

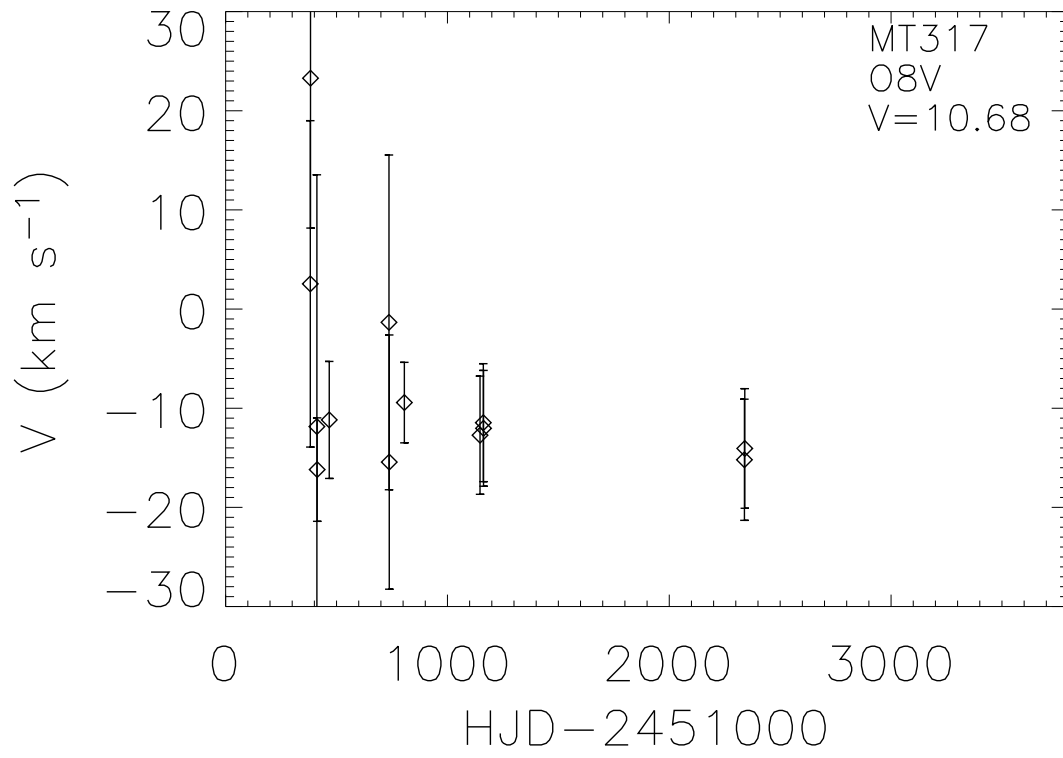


Fig. 16.— Relative radial velocity variation for MT317, a system with little or no variation.

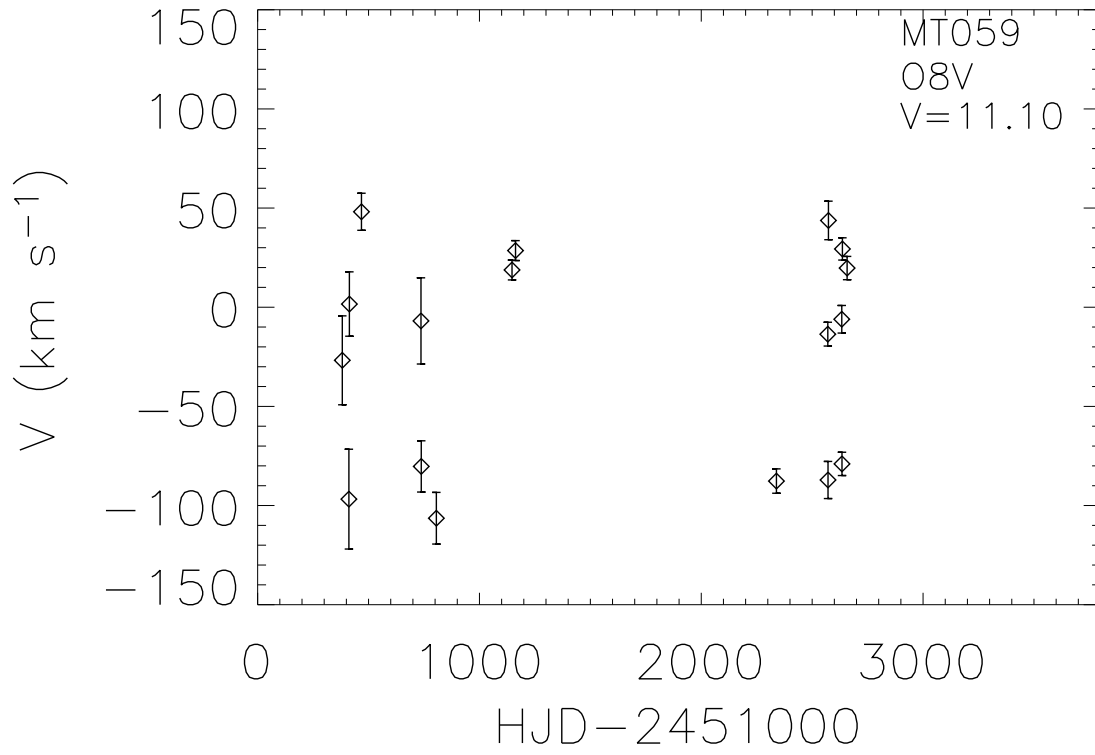


Fig. 17.— Relative radial velocity variation for MT059, one of the more prominent velocity-variable systems. MT059 is among the 36 stars with $P(\chi^2, \nu) \leq 0.01$.

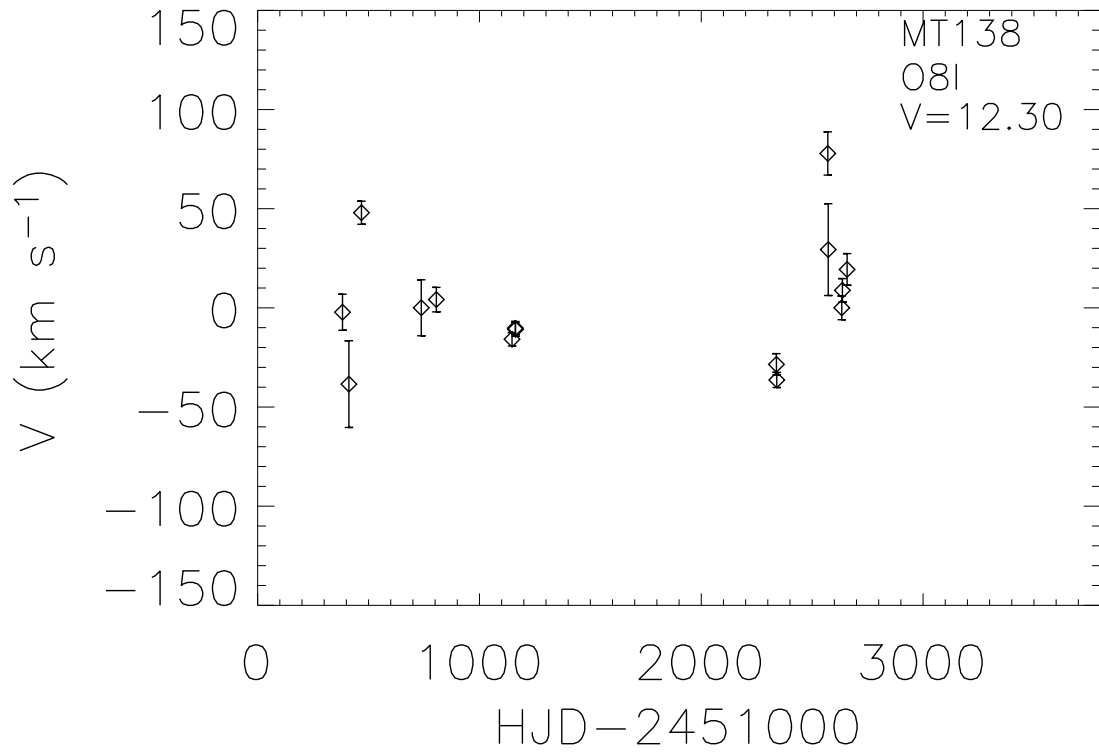


Fig. 18.— Relative radial velocity variation for MT138, one of the more prominent velocity-variable systems.

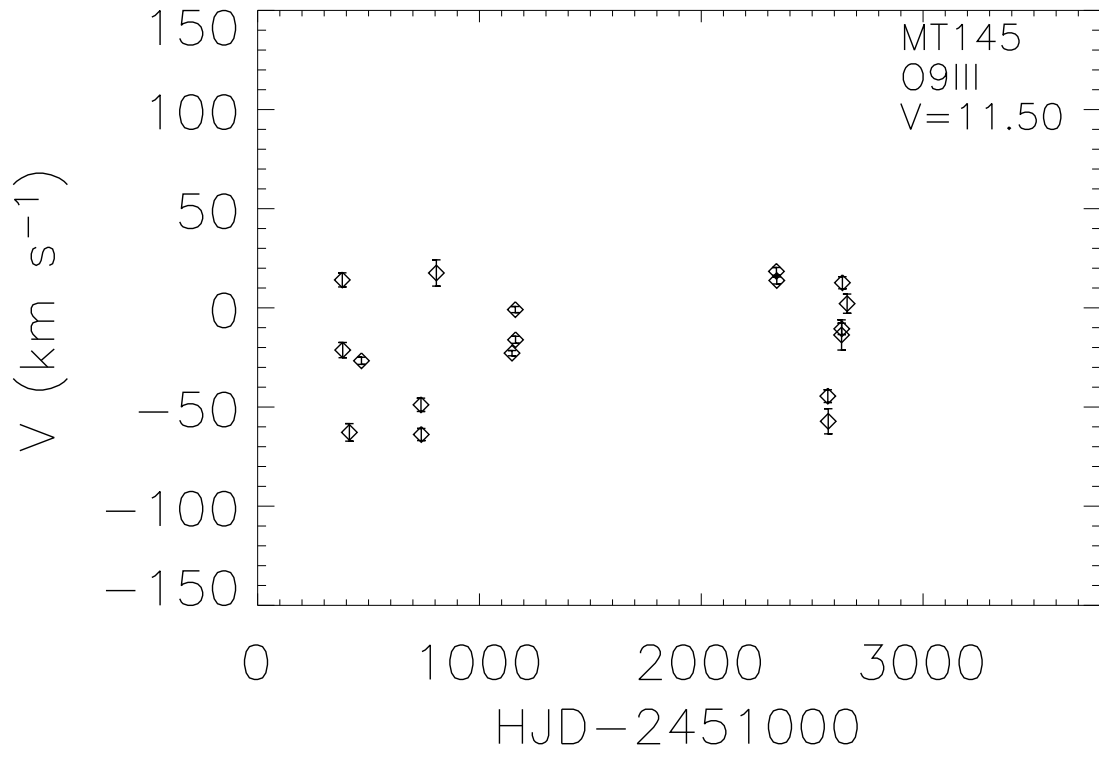


Fig. 19.— Relative radial velocity variation for MT145, one of the more prominent velocity-variable systems.

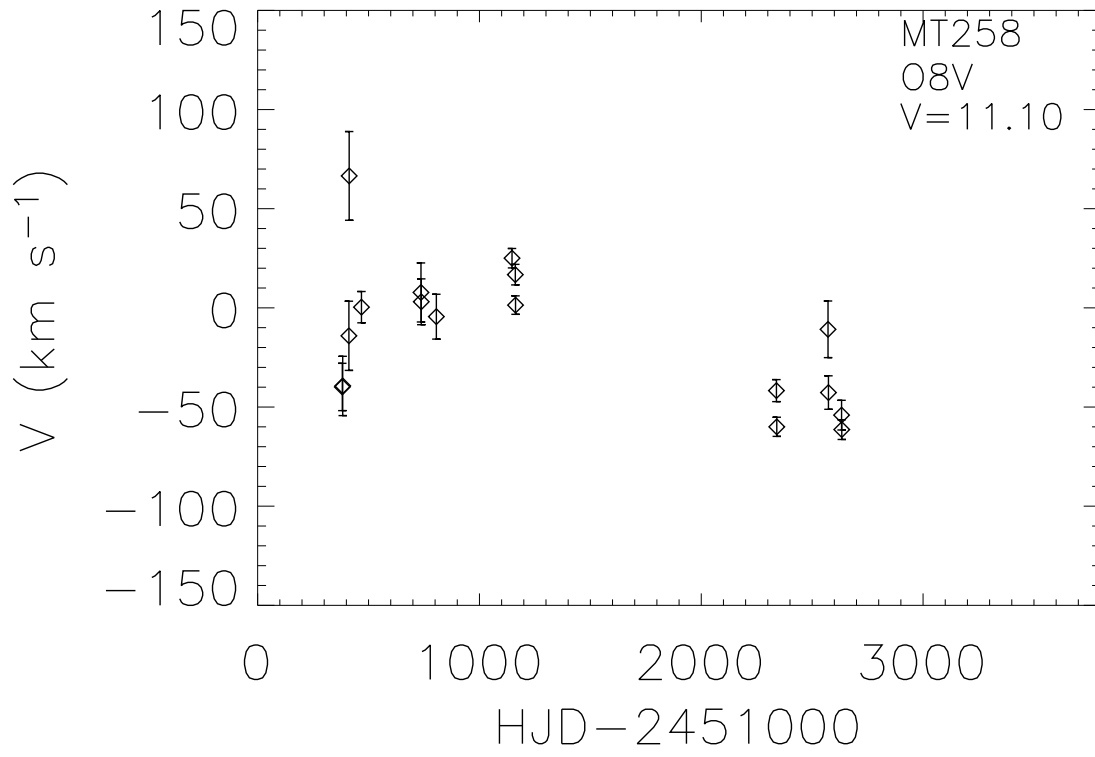


Fig. 20.— Relative radial velocity variation for MT258, one of the more prominent velocity-variable systems.

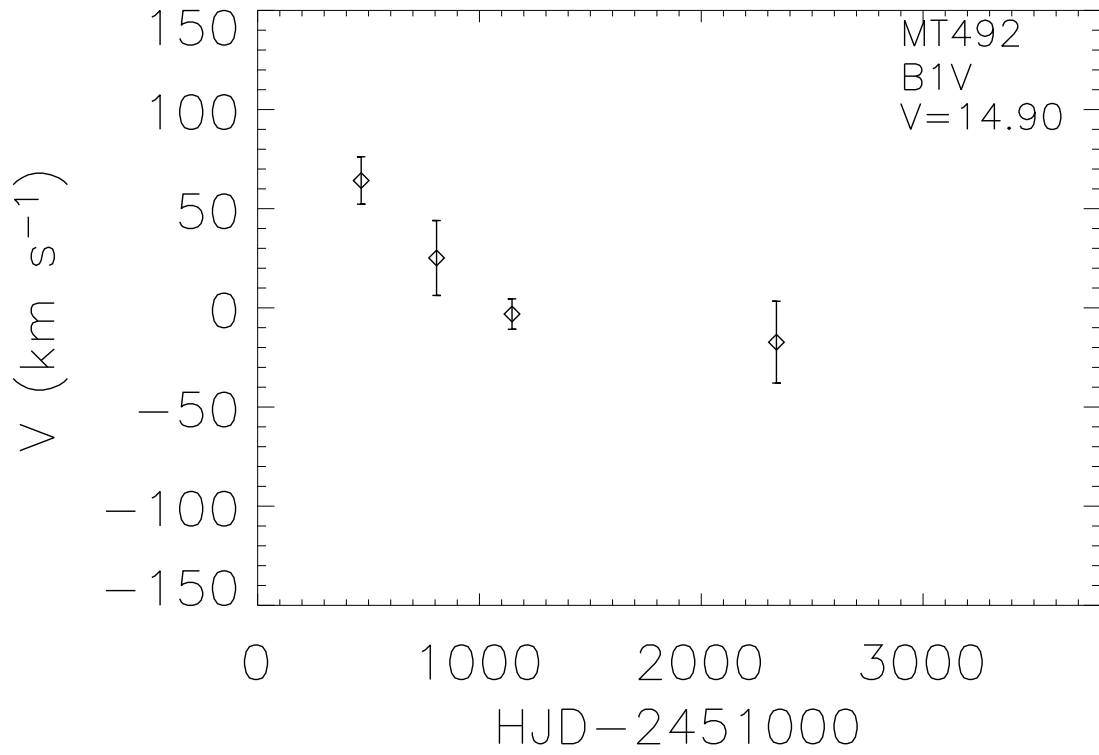


Fig. 21.— Relative radial velocity variation for MT492, one of the more prominent velocity-variable systems.

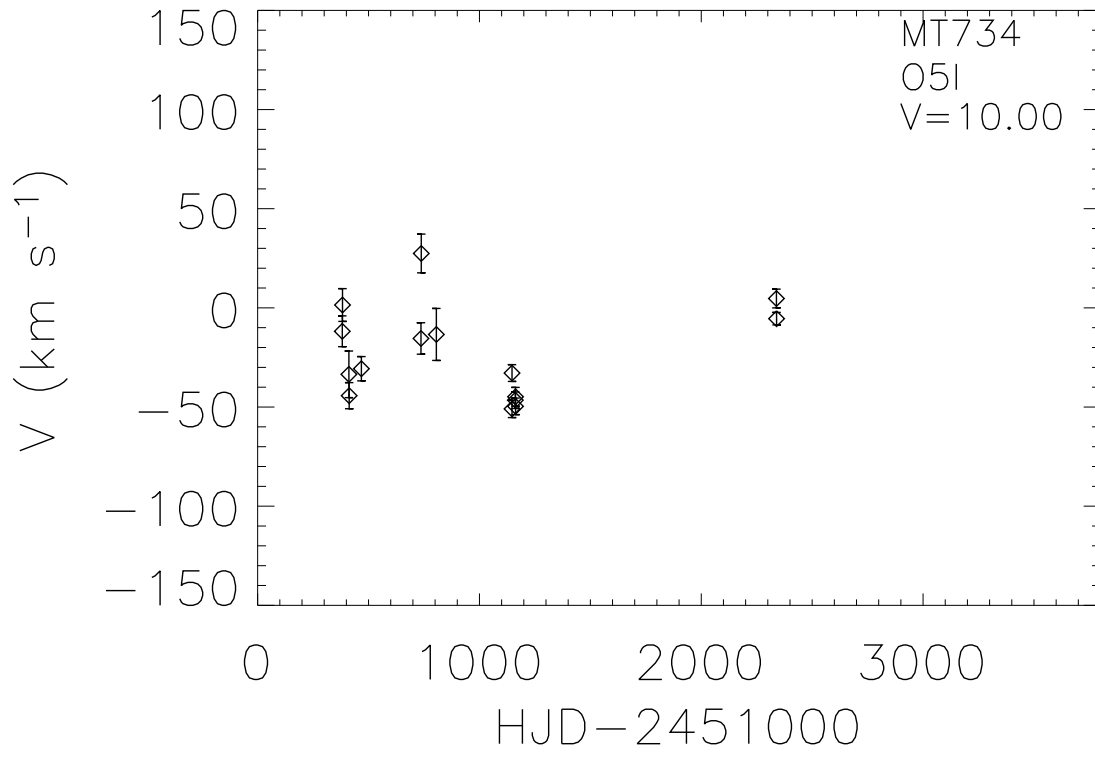


Fig. 22.— Relative radial velocity variation for MT734, one of the more prominent velocity-variable systems.

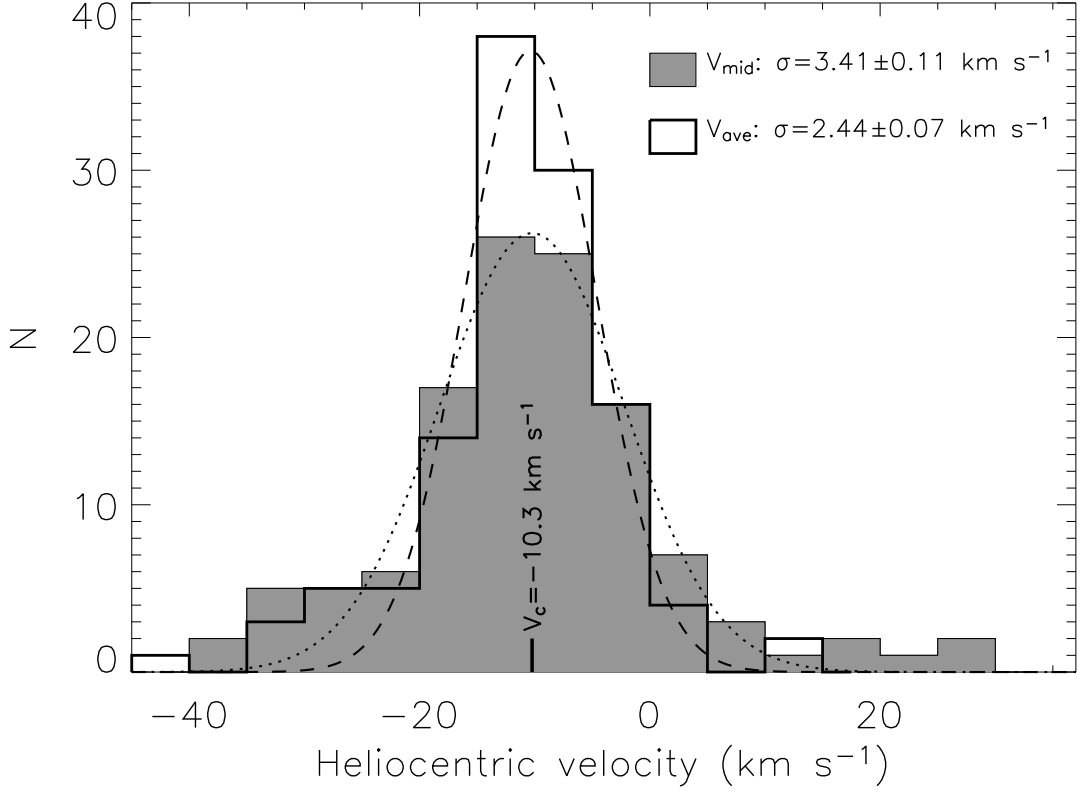


Fig. 23.— Mean systemic velocity distribution for Cygnus OB2 stars listed in Table 5. The unshaded histogram represents the V_{avg} velocities in column 4. The shaded histogram represents the V_{mid} velocities from column 5. Gaussian fits to each histogram yield a mean systemic velocity of $\sim -10 \text{ km s}^{-1}$, and dispersions of $\sigma = 2.44 \pm 0.07 \text{ km s}^{-1}$ for V_{avg} and $\sigma = 3.41 \pm 0.11$ for V_{mid} .